

1     **Landsat and Sentinel-derived glacial lake dataset in the China-**  
2             **Pakistan Economic Corridor from 1990 to 2020**

3  
4     Muchu Lesi<sup>1</sup>, Yong Nie<sup>1, \*</sup>, Dan H. Shugar<sup>2</sup>, Jida Wang<sup>3</sup>, Qian Deng<sup>1, 4</sup>, Huayong Chen<sup>1</sup>,  
5     Jianrong Fan<sup>1</sup>

6  
7     <sup>1</sup>Institute of Mountain Hazards and Environment, Chinese Academy of Sciences, Chengdu,  
8     China

9     <sup>2</sup>Water, Sediment, Hazards, and Earth-surface Dynamics (waterSHED) Lab, Department of  
10     Geoscience, University of Calgary, Alberta, T2N 1N4, Canada

11     <sup>3</sup>Department of Geography and Geospatial Sciences, Kansas State University, Manhattan,  
12     Kansas 66506, USA

13     <sup>4</sup>University of Chinese Academy of Sciences, Beijing 100190, China

14  
15  
16  
17     \*Corresponding author, [nieyong@imde.ac.cn](mailto:nieyong@imde.ac.cn)  
18  
19

20 **Abstract.** The China-Pakistan Economic Corridor (CPEC) is one of the flagship projects of  
21 the One Belt One Road Initiative, which faces threats from water shortage and mountain  
22 disasters in the high-elevation region, such as glacial lake outburst floods (GLOFs). An up-to-  
23 date high-quality glacial lake dataset with parameters such as lake area, volume, and type,  
24 which is fundamental to water resource and flood risk assessments, and predicting glacier-  
25 lake evolutions, is still largely absent for the entire CPEC. This study describes a glacial lake  
26 dataset for the CPEC using a threshold-based mapping method associated with rigorous  
27 visual inspection workflows. This dataset includes (1) multi-temporal inventories for 1990,  
28 2000, and 2020 produced from 30 m resolution Landsat images, and (2) a glacial lake  
29 inventory for the year 2020 at 10 m resolution produced from Sentinel-2 images. The results  
30 show that, in 2020, 2234 lakes were derived from the Landsat images, covering a total area of  
31  $86.31 \pm 14.98 \text{ km}^2$  with a minimum mapping unit of 5 pixels ( $4500 \text{ m}^2$ ), whereas 7560 glacial  
32 lakes were derived from the Sentinel-2 images with a total area of  $103.70 \pm 8.45 \text{ km}^2$  with a  
33 minimum mapping unit of 5 pixels ( $500 \text{ m}^2$ ). The discrepancy shows that Sentinel-2 can  
34 detect a significant quantity of smaller lakes than Landsat due to its finer spatial resolution.  
35 Glacial lake data in 2020 was validated by Google Earth-derived lake boundaries with a  
36 median ( $\pm$ standard deviation) difference of  $7.66 \pm 4.96 \%$  for Landsat-derived product and  
37  $4.46 \pm 4.62 \%$  for Sentinel-derived product. The total number and area of glacial lakes from  
38 consistent 30 m resolution Landsat images remain relatively stable despite a slight increase  
39 from 1990 to 2020. A range of critical attributes has been generated in the dataset, including  
40 lake types and mapping uncertainty estimated by an improved Hanshaw's equation. This  
41 comprehensive glacial lake dataset has the potential to be widely applied in studies on water  
42 resource assessment, glacial lake-related hazards, and glacier-lake interactions, and is freely  
43 available at <https://doi.org/10.12380/Glaci.msdc.000001> (Lesi et al., 2022).

## 44 **1 Introduction**

45 Glaciers in High-mountain Asia (HMA) play a crucial role in regulating climate, supporting  
46 ecosystems, modulating the release of freshwater into rivers, and sustaining municipal water  
47 supplies (Wang et al., 2019; Viviroli et al., 2020), agricultural irrigation, and hydropower  
48 generation (Pritchard, 2019; Nie et al., 2021). Most HMA glaciers are losing mass in the  
49 context of climate change (Brun et al., 2017; Maurer et al., 2019; Shean et al., 2020;  
50 Bhattacharya et al., 2021), therefore, unsustainable glacier melt and the passing of peak water  
51 are reducing the hydrological role of glaciers (Huss and Hock, 2018) and impacting  
52 downstream ecosystem services, agriculture, hydropower and other socioeconomic values  
53 (Carrivick and Tweed, 2016; Nie et al., 2021). The present and future glacier changes not  
54 only impact the water supply for the downstream area but also alter the frequency and  
55 intensity of glacier-related hazards, such as glacier lake outburst floods (GLOFs) (Nie et al.,  
56 2018; Rounce et al., 2020; Zheng et al., 2021), and rock and ice avalanches (Shugar et al.,  
57 2021). Global glacial lake number and total area both increased between 1990 and 2018 in  
58 response to glacier retreat and climate change (Shugar et al., 2020), affecting the allocation of  
59 freshwater resources. The Indus is globally the most important and vulnerable water tower  
60 unit where glaciers, lakes, and reservoir storage contribute about two-thirds of the water  
61 supply (Immerzeel et al., 2020). Ice-marginal lakes store  $\sim 1\%$  of total ice discharge in  
62 Greenland and accelerate lake-terminating ice velocity by  $\sim 25\%$  (Carrivick et al., 2022). An

63 increasing frequency and risk of GLOFs (Nie et al., 2021; Zheng et al., 2021) is threatening  
64 the Asian population and infrastructures in the mountain ranges, such as the China-Pakistan  
65 Economic Corridor (CPEC), as a flagship component of One Belt One Road Initiative  
66 (Battamo et al., 2021; Li et al., 2021). The northern section of the CPEC passes through  
67 Pamir, Karakoram, Hindu Kush, and Himalaya mountains where droughts and glacier-related  
68 hazards are frequent and severe (Hewitt, 2014; Bhambri et al., 2019; Pritchard, 2019),  
69 threatening local people, the existing, under-construction and planned infrastructures, such as  
70 highways, hydropower plants, and railways. Understanding the risk posed by water shortage  
71 and glacier-related hazards is a critical step toward sustainable development for the CPEC.

72 Glacial lake inventories with a range of attributes benefit water resource assessment and  
73 disaster risk assessment related to glacial lakes (Wang et al., 2020; Carrivick et al., 2022),  
74 and contribute to predicting glacier-lake evolution and cryosphere-hydrosphere interactions  
75 under climate change (Nie et al., 2017; Brun et al., 2019; Maurer et al., 2019; Carrivick et al.,  
76 2020; Liu et al., 2020). Remote sensing is the most viable way to map glacial lakes and detect  
77 their spatio-temporal changes in the high-elevation zones where in situ accessibility is  
78 extremely low (Huggel et al., 2002; Quincey et al., 2007). Studies in glacial lake inventories  
79 using satellite observations have been heavily conducted at regional scales recently, such as  
80 in the Tibetan Plateau (Zhang et al., 2015), the Himalaya (Gardelle et al., 2011; Nie et al.,  
81 2017), the HMA (Wang et al., 2020; Chen et al., 2021), the Tien Shan (Wang et al., 2013),  
82 the Alaska (Rick et al., 2022), the Greenland (How et al., 2021) and the northern Pakistan  
83 (Ashraf et al., 2017). However, the latest glacial lake mapping in 2020 is still absent along the  
84 CPEC. Among existing studies, Landsat archival images are the most widely used due to their  
85 multi-decadal record of earth surface observations, reasonably high spatial resolution (30 m),  
86 and publicly available distribution (Roy et al., 2014). Freely available Sentinel-2 satellite  
87 images show a better potential than Landsat in glacial lake mapping and inventories due to  
88 their higher spatial resolution (10 m) and global coverage, but have only been available since  
89 late 2015 (Williamson et al., 2018; Paul et al., 2020). Glacial lake inventories using Sentinel-  
90 2 images are relatively scarce at regional scales, and studies of the latest glacial lake mapping  
91 as well as comparisons of glacial lake datasets derived from Sentinel-2 and Landsat  
92 observations are still lacking.

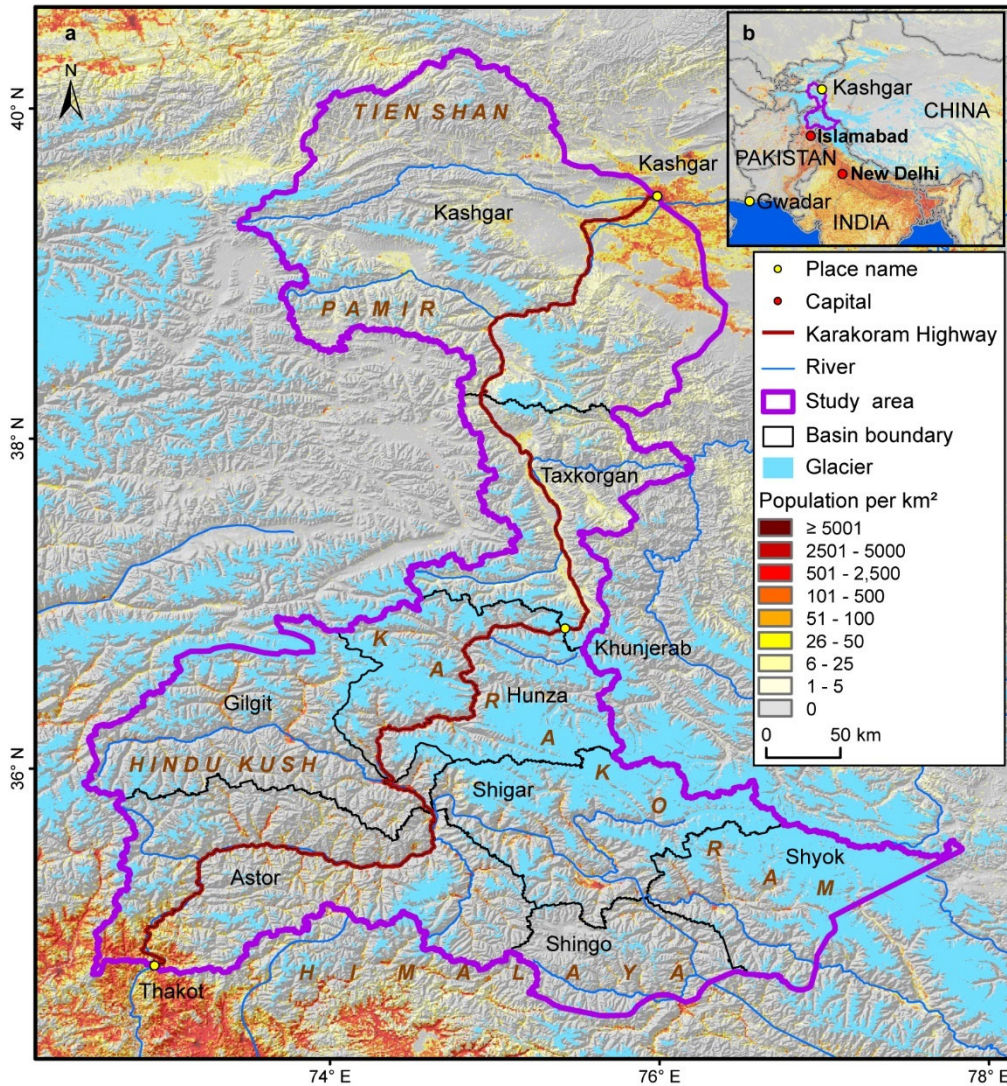
93 Discrepancies between various glacial lake inventories (Zhang et al., 2015; Shugar et al.,  
94 2020; Wang et al., 2020; Chen et al., 2021; How et al., 2021) result from differences in  
95 mapping methods, minimum mapping units, the definition of glacial lakes, periods, data  
96 sources and other factors. For example, the manual vectorization method was widely adopted  
97 at the earlier stage for its high accuracy. However, it is time-consuming associated with high  
98 labor intensity, and is only practical at regional scales (Zhang et al., 2015; Wang et al., 2020).  
99 Automated and semi-automated lake mapping methods, such as multi-spectral index  
100 classification (Gardelle et al., 2011; Nie et al., 2017; Zhang et al., 2018; How et al., 2021),  
101 have been developed to improve the efficiency of glacial lake inventories using optical  
102 images, although manual modification is often unavoidable to assure the quality of lake data  
103 impacted by cloud cover, mountain shadows, seasonal snow cover and frozen lake surfaces  
104 (Sheng et al., 2016; Wang et al., 2017, 2018). Backscatter images from Synthetic Aperture  
105 Radar (SAR) (Wangchuk and Bolch, 2020; How et al., 2021) were used to remove the impact  
106 of cloud cover for lake mapping. Besides, other approaches such as hydrological sink

107 detection using DEM (How et al., 2021) and land surface temperature-based detection  
108 method (Zhao et al., 2020) were also used for lake inventories. Different classification  
109 methods impact the results of lake mapping and monitoring. So far, we are lacking a unified  
110 standard for the classification system of glacial lakes (Yao et al., 2018). Existing  
111 classification systems are generally used for their research purposes, mainly based on the  
112 relative positions of glacial lakes and glaciers, the supply conditions of glaciers, and the  
113 attributes of dams. In addition to different classification standards, the same type of glacial  
114 lakes may also have different names given by different scholars. For example, ice-marginal  
115 (Carrivick and Quincey, 2014; Carrivick et al., 2020), ice-contact (Carrivick and Tweed,  
116 2013), and proglacial (Nie et al., 2017) lakes all represent glacial lakes sharing the boundary  
117 with glaciers. Glacier lakes in currently available datasets have been traditionally categorized  
118 by their spatial relationship with upstream glaciers (Gardelle et al., 2011; Wang et al., 2020;  
119 Chen et al., 2021), and classification attributes considering the formation mechanism and the  
120 properties of dams are rare or incomplete in the CPEC (Yao et al., 2018; Li et al., 2020).  
121 Dam-type classification of glacial lakes provides a crucial attribute for glacier-lake  
122 interactions and risk assessment (Emmer and Cuřín, 2021). Therefore, an up-to-date glacial  
123 lake dataset with critical, quality-assured parameters (e.g. lake area, volume, and type) is  
124 necessary.

125 This study aims to (1) present an up-to-date glacial lake dataset in the CPEC in 2020 using  
126 both Landsat 8 and Sentinel-2 images to accurately document its detailed lake distribution;  
127 (2) present two historical glacial lake datasets for the CPEC to show the extent in 1990 and  
128 2000 using consistent 30-m Landsat images to reveal glacial lake changes at three time  
129 periods (1990, 2000 and 2020); and (3) generate a range of critical attributes for glacial lake  
130 inventories to benefit studies on water resource evaluation, risk assessment of GLOFs, glacier  
131 –lake evolution modeling in the HMA.



132 **2 Study area**



133  
 134 **Figure 1.** Location of the study area associated with the distribution of glaciers (RGI Consortium, 2017),  
 135 mountains, basins, and population (Rose et al., 2021) (a), and its location within the CPCE (b).  
 136

137 The northern part of the CPCE is selected as the study area (Figure 1). The CPCE, originating  
 138 from Kashgar of the Xinjiang Uygur Autonomous region, China and extending to Gwadar Port,  
 139 Pakistan (Ullah et al., 2019; Yao et al., 2020), is connecting China and Pakistan via the only  
 140 Karakoram Highway. The study area covers all the drainage basins along Karakoram Highway  
 141 starting from Kashgar and ending at Thakot, with a total area of ~125,000 km<sup>2</sup>. The upper Indus  
 142 basins beyond the Pakistani-administrated border are excluded from this study due to the spatial  
 143 coverage of the CPCE. The entire study area is divided into eight sub-basins, covering most of  
 144 the Karakoram with the highest elevation up to 8611 m, western Himalaya and Tien Shan,  
 145 eastern Hindu Kush, and the Pamir Mountains. The 9710 glaciers in the study area cover a total  
 146 area of 17,447 km<sup>2</sup> and nearly 60% of glaciers are distributed in the Karakoram (5818 glaciers  
 147 with a total area of 14,067.52 km<sup>2</sup>) (RGI Consortium, 2017). Most glaciers in the western  
 148 Himalaya and eastern Hindu Kush are losing mass in the context of climate change (Kääb et

149 al., 2012; Yao et al., 2012; Brun et al., 2017; Shean et al., 2020; Hugonnet et al., 2021), whereas  
150 the glaciers in the eastern Karakoram and Pamir have shown unusually little changes, including  
151 unchanged, retreated, advanced and surged glaciers (Hewitt, 2005; Kääb et al., 2012; Bolch et  
152 al., 2017; Brun et al., 2017; Shean et al., 2020; Nie et al., 2021). The spatially heterogeneous  
153 distribution and changes of glaciers are primarily explained as a result of differences in the  
154 dominant precipitation-bearing atmospheric circulation patterns that include the winter  
155 westerlies the Indian summer monsoon, their changing trends, and their interactions with local  
156 extreme topography (Yao et al., 2012; Azam et al., 2021; Nie et al., 2021).

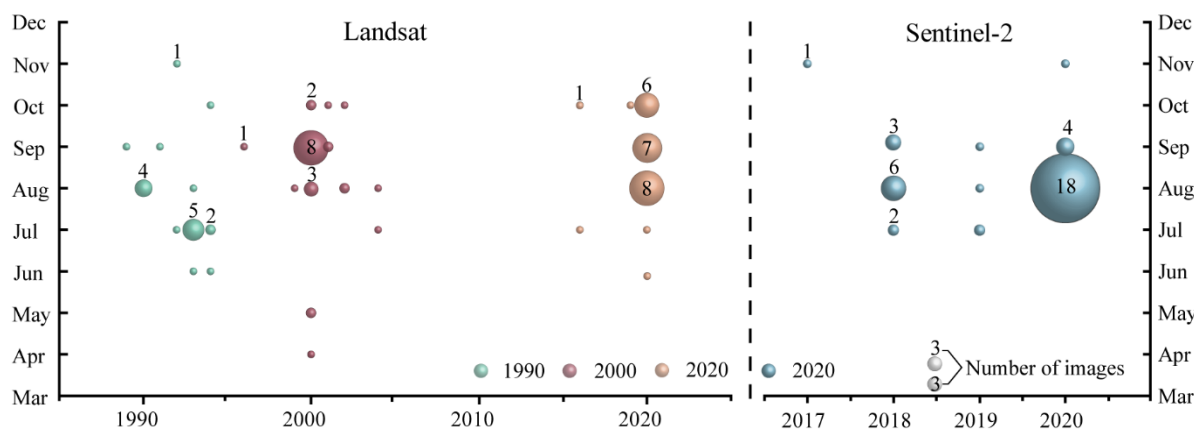
### 157 **3 Data sources**

158 Both Landsat and Sentinel-2 images have been employed to map glacial lakes between 1990  
159 and 2020 in the CPEC (Figure 2). A total number of 71 Landsat Thematic Mapper (TM),  
160 Thematic Mapper Plus (ETM+), and Landsat 8 Operational Land Imager (OLI) images with a  
161 consistent spatial resolution of 30 m were downloaded from the United States Geological  
162 Survey Global Visualization Viewer (GloVis, <https://glovis.usgs.gov/>) to be used to create  
163 glacial lake inventories in 1990, 2000 and 2020. High-quality Landsat-5 images around 2010  
164 are insufficient to cover the entire study area, so we were unable to map lakes in 2010 due to  
165 Landsat-7's scan-line corrector errors and significant cloud covers. In addition, 39 Sentinel-2  
166 images (23 scenes in 2020) were downloaded from Copernicus Open Access Hub  
167 (<https://scihub.copernicus.eu/>) to produce the 10-m resolution glacial lake inventory in 2020.  
168 All images used in this study have been orthorectified before download, but we still find that  
169 one Sentinel-2 image was not well matched with Landsat images, leading to the discrepancy  
170 between the two glacial lake datasets. We manually georeferenced the shifted image to  
171 minimize the difference between Sentinel- and Landsat-derived glacial lakes.

172 Cloud and snow covers heavily affect the usability of optical satellite images (Wulder et  
173 al., 2019) and their availability in the entire study area, so we took advantage of the images  
174 acquired before and after each of the baseline years 1990, 2000 and 2020 to construct the  
175 glacial lake inventories. Only 4 images in 1990 (the largest covering the study area), 16  
176 images in 2000, and 23 images in 2020 were used for matching baseline year. Spatially, high-  
177 quality images in given baseline years were preferentially chosen, or we selected one or more  
178 alternative images acquired in adjacent years to delineate glacial lakes by removing the effect  
179 of cloud and snow covers. To minimize the impact of intra-annual changes on glacial lakes,  
180 most of the used images (82% for Sentinel-2 and 75% for Landsat) were acquired from  
181 August to October in the given baseline year with cloud coverage of <20% for each image.  
182 For some specific scenes where cloud cover exceeded the threshold of 20%, we selected  
183 more than one image to remedy the effect of cloud contamination (Nie et al., 2010, 2017;  
184 Jiang et al., 2018).

185 Other datasets used include the Randolph Glacier Inventory version 6.0 (Pfeffer et al.,  
186 2014; RGI Consortium, 2017) and the Glacier Area Mapping for Discharge from the Asian  
187 Mountains (GAMDAM) glacier inventory (Sakai, 2019). These two glacier datasets were  
188 used to determine glacial lake types, such as ice-contact, ice-dammed, and unconnected-  
189 glacier-fed lakes. The Shuttle Radar Topography Mission Digital Elevation Model (SRTM  
190 DEM) at a 1-arc second (30 m) resolution (Jarvis et al., 2008) was employed to extract the  
191 altitudinal characteristics of the glacial lakes. The absolute vertical accuracy of the SRTM

192 DEM is 16 m (90%) (Rabus et al., 2003; Farr et al., 2007). We also applied other published  
 193 glacial lake datasets for comparative analysis. They include the glacial lake inventories of  
 194 HMA in 1990 and 2018 downloaded from <http://doi.org/10.12072/casnw.064.2019.db> (Wang  
 195 et al., 2020), the Third Pole region in 1990, 2000, and 2010 publicly shared at  
 196 <http://en.tpdatabase.cn/> (Zhang et al., 2015), the Tibet Plateau from 2008 to 2017 accessed at  
 197 <https://doi.org/10.5281/zenodo.3700282> (Chen et al., 2021), and the entire world in 1990,  
 198 2000 and 2015 provided at [https://nsidc.org/data/HMA\\_GLI/versions/1](https://nsidc.org/data/HMA_GLI/versions/1) (Shugar et al.,  
 199 2020). In addition, field survey data collected between 2017 and 2018 were also used to assist  
 200 in lake mapping and glacial lake type classification.  
 201



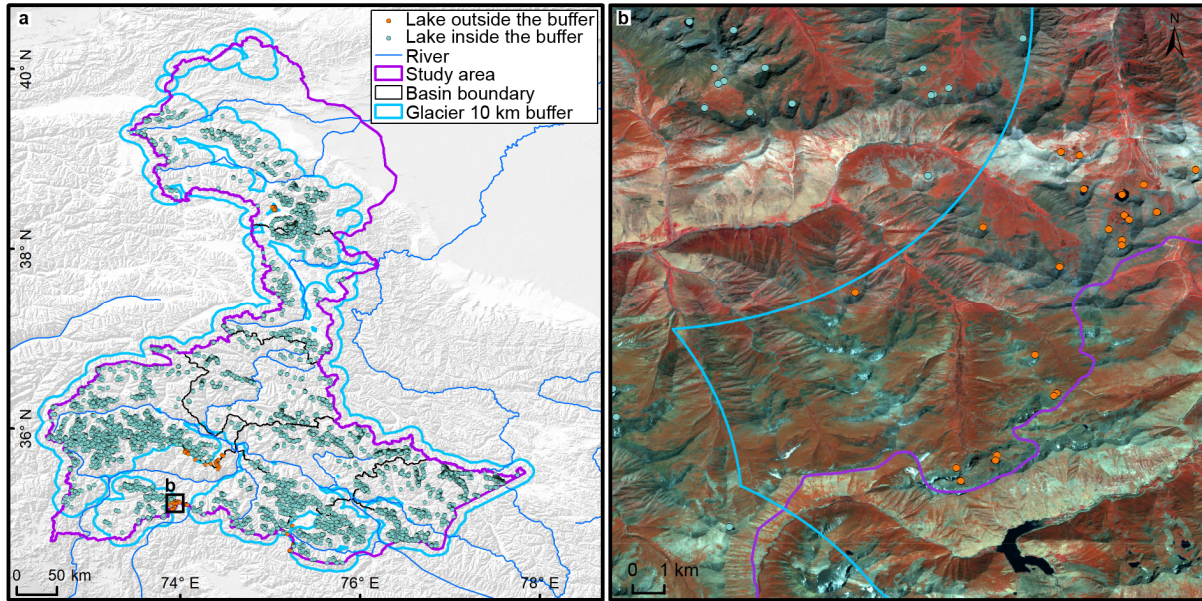
202  
 203 **Figure 2.** Acquisition of years and months of Landsat and Sentinel-2 images selected for glacial lake  
 204 inventories. The bubble size indicates the available high-quality image number.

## 205 4 Glacial lake inventory methods

### 206 4.1 Definition of glacial lakes

207 We consider a glacial lake as one that formed as a result of modern or ancient glaciation.  
 208 Contemporary glacial lakes are easily recognized using a combination of glacier inventories  
 209 and remote sensing images. Ancient glacial lakes can be identified from periglacial  
 210 geomorphological characteristics, including moraine remnants and U-shaped valleys that are  
 211 discernible from satellite observations (Post and Mayo, 1971; Westoby et al., 2014; Nie et al.,  
 212 2018; Martín et al., 2021). A 10-km buffering distance of RGI 6.0 glacier boundaries that has  
 213 been widely used in previous studies (Zhang et al., 2015; Wang et al., 2020), was created to  
 214 help map glacial lakes. A few glacial lakes in the study area (a total of 84 lakes for the  
 215 Sentinel-2 dataset and 55 lakes for the Landsat dataset in 2020) beyond the buffering zone,  
 216 located near buffering boundaries, were intentionally included due to clear evidence of  
 217 glaciation (Figure 3). Landslide-dammed lakes (Chen et al., 2017) in the buffering zone were  
 218 excluded from our inventories because of their irrelevance to glaciation. All glacial lakes in  
 219 the study area were mapped according to our definition. We were able to implement this  
 220 definition by carefully leveraging the spectral properties of glacial lakes and the periglacial  
 221 geomorphological features that are often evident in remote sensing images (see more in  
 222 sections 4.3 and 4.4).  
 223





224  
225  
226  
227

**Figure 3.** The 10-km buffer zone of RGI 6.0 glacier boundaries (a) and Sentinel-derived glacial lakes located near buffering boundary within the study area (b).

#### 228 4.2 Interactive lake mapping

229 A human-interactive and semi-automated lake mapping method (Wang et al., 2014; Nie et al.,  
230 2017, 2020) was adopted to accurately extract glacial lake extents using Landsat and  
231 Sentinel-2 images, based on the Normalized Difference Water Index (NDWI) (Mcfeeters,  
232 1996). The NDWI uses the green and near-infrared bands and is calculated by the following  
233 equation:

$$234 \quad NDWI = \frac{Band_{Green} - Band_{NIR}}{Band_{Green} + Band_{NIR}} \quad (1)$$

235 where the green band and near-infrared band were provided by both Landsat and Sentinel  
236 multispectral images.

237 Specifically, the method calculated the NDWI histogram based on the pixels with each  
238 user-defined and manually-drawn region of interest. The NDWI threshold that separates the  
239 lake surface from the land was interactively determined by screening the NDWI histogram  
240 against the lake region in the imagery (Wang et al., 2014; Nie et al., 2020). This way, the  
241 determined NDWI threshold can be well-tuned to adapt to various spectral conditions of the  
242 studied glacial lakes. The raster lake extents segmented by the thresholds were then  
243 automatically converted to vector polygons. We first completed the glacial lake inventory in  
244 2020 using this interactive mapping method, and the 2020 inventory was then used as a  
245 reference to facilitate the lake mapping for other periods.

246 The minimum mapping unit (MMU) was set to 5 pixels for both Landsat (0.0045 km<sup>2</sup>) and  
247 Sentinel-2 images (0.0005 km<sup>2</sup>) in this study. MMU determines the total number and area of  
248 glacial lakes in the dataset and varies in the previous studies, such as 3 pixels (Zhang et al.,  
249 2015), 6 pixels (Wang et al., 2020), or 9 pixels (Chen et al., 2021) for a regional scale, or 55  
250 pixels (Shugar et al., 2020) for a global scale. While a smaller threshold leads to a large  
251 number of lakes mapped, it also generates larger mapping noises or uncertainties.

252 Considering this signal-noise balance and our focus on identifying prominent glacier lake  
253 dynamics in the study area, we opted to use 5 pixels as the MMU for both Landsat and  
254 Sentinel-2 images.

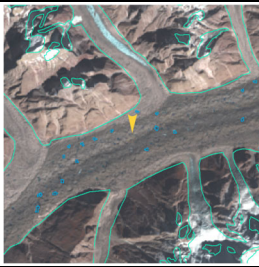


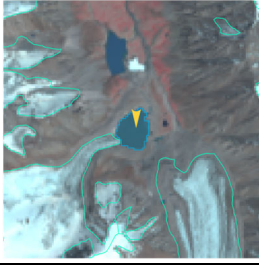
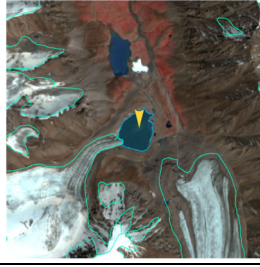

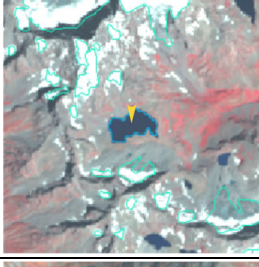
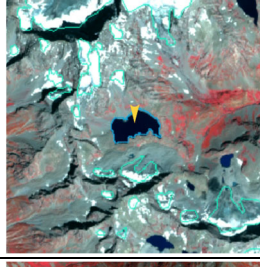
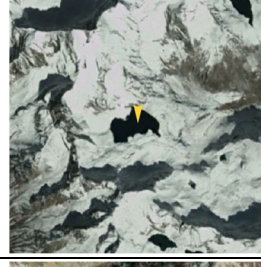

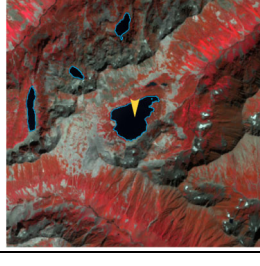

255 Several procedures were taken to assure the quality assurance and quality control for lake  
256 mapping, including 1) visual inspection and modification using the threshold-based mapping  
257 method for each lake according to Landsat, Sentinel-2, and Google Earth high-resolution  
258 images overlaying preliminarily lake boundary extraction at the given period; 2) time series  
259 check for Landsat-derived glacial lake datasets from 1990 and 2020, and cross-check  
260 between Landsat and Sentinel-2-derived lake dataset in 2020 to reduce errors of omission and  
261 commission; 3) topological validation of glacial lake mapping, such as repeated removal,  
262 elimination of small sliver polygons; and 4) logical check for lake types between two  
263 classification systems of glacial lakes. False lake extents resulting from cloud or snow cover,  
264 lake ice, and topographic shadows (Nie et al., 2017, 2020) were modified using the previous  
265 semi-automated mapping method based on alternative images acquired in adjacent years.  
266 Those procedures were time-consuming but helped to minimize the effect of cloud and snow  
267 covers, and lake mapping errors, and to maximize the quality of the produced lake product  
268 and the derived glacial lake changes.

#### 269 4.3 Classification of glacial lakes

270 Two glacial lake classification systems (GLCS) have been established based on the  
271 relationship of interaction between glacial lakes and glaciers as well as lake formation  
272 mechanism and dam material properties. In the first GLCS (GLCS1), glacial lakes were  
273 classified into four types based on their spatial relationship to upstream glaciers: supraglacial,  
274 ice-contact, unconnected-glacier-fed lakes, and non-glacier-fed lakes according to Gardelle et  
275 al. (2011) and Carrivick et al. (2013). Alternatively, combining the formation mechanism of  
276 glacial lakes and the properties of natural dam features, glacial lakes were classified into five  
277 categories (herein named GLCS2) modified from Yao's classification system (2018):  
278 supraglacial, end-moraine-dammed, lateral-moraine-dammed, glacial-erosion lakes and ice-  
279 dammed lakes. Subglacial lakes were excluded due to the mapping challenge from spectral  
280 satellite images alone. Characterization and examples for each type are provided in Table 1  
281 and Table 2. Individual glacial lakes were categorized into the specific types for each GLCS  
282 according to available glacier inventory data, and geomorphological and spectral  
283 characteristics interpreted from Landsat, Sentinel, and Google Earth images. The synergy of  
284 these two GLCSs is beneficial to predicting glacier-lake evolutions and providing  
285 fundamental data for water resource and glacial lake disaster risk assessment.

286



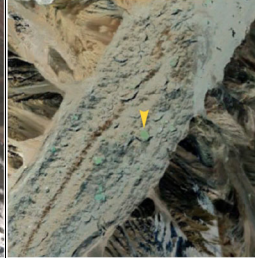
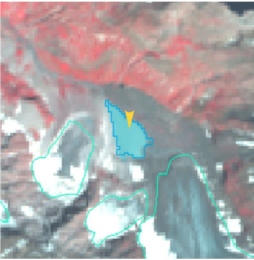
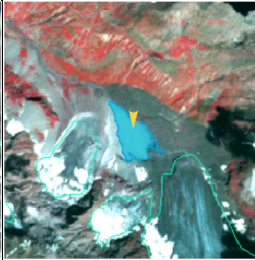





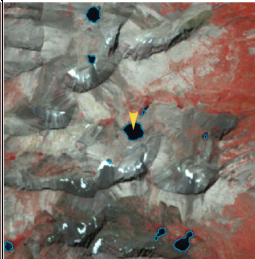


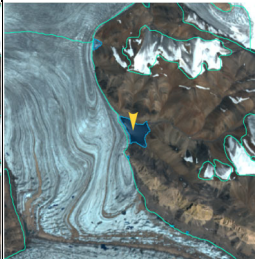
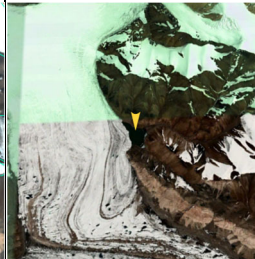
287 **Table 1.** A classification system of glacial lake types (GLCS1) according to the relationship between  
 288 glacial lakes and glaciers (© Google Earth 2019). Glacier outlines are from RGI 6.0 (RGI Consortium,  
 289 2017), and the yellow marker represents the target lake.

| Lake types              | Characteristics   | Landsat   | Sentinel-2   | Google Earth  |
|-------------------------|---|---|--|---|
| Supraglacial            | Lakes formed on the surface of glaciers, generally dammed by ice and thin debris.<br><br>Case location:<br>35°43'49.74" N<br>76°13'53.88" E                               |    |    |    |
| Ice-contact             | Lakes are dammed by moraine, ice, or bedrock, supplied by glacial meltwater, and shared boundary with glaciers.<br><br>Case location:<br>39°09'32.40" N<br>73°43'12.00" E |    |    |    |
| Unconnected-glacier-fed | Lakes are currently supplied by upstream glacial meltwater but disconnected from glaciers.<br><br>Case location:<br>35°47'60.00" N<br>72°55'15.60" E                      |   |   |   |
| Non-glacier-fed         | Lakes formed by glaciology, dammed by moraine or bed rock, and currently not supplied by glacial meltwater.<br><br>Case location:<br>34°50'39.99" N<br>74°48'29.31" E     |  |  |  |

290



291 **Table 2.** A classification system of glacial lake types (GLCS2) according to the formation mechanism of  
 292 glacial lakes and dam material properties (© Google Earth 2019). The glacier outlines from RGI 6.0 (RGI  
 293 Consortium, 2017), and the yellow marker represents the target lake.

| Lake types             | Characteristics  | Landsat   | Sentinel-2   | Google Earth  |
|------------------------|--|---|--|---|
| Supraglacial           | Lakes formed on the surface of glaciers, generally dammed by ice and thin debris.<br><br>Case location:<br>36°46'7.39" N<br>74°20'7.59" E  |    |    |    |
| End-moraine-dammed     | Lakes formed behind moraines as a result of glacier retreat and downwasting.<br><br>Case location:<br>35°42'50.40" N<br>73°09'57.60" E   |    |    |    |
| Lateral-moraine-dammed | Lakes formed behind lateral glacial moraine ridges and are dammed by debris, different from an ice-dammed glacial lake.<br><br>Case location:<br>38°28'45.62" N<br>75°20'52.30" E  |   |   |   |
| Glacial-erosion        | Lakes formed in depressions created by glacial over-deepening. Bedrock dam dominates, partially superimposed by top moraine in rugged terrain. Dams are unclear in the satellite images.<br>Case location:<br>35°55'55.56" N<br>73°38'20.13" E |  |  |  |
| Ice-dammed             | Lakes formed behind glaciers, dammed by glacier ice (partially covered by debris on the top).<br><br>Case location:<br>35°28'31.32" N<br>77°30'46.81" E  |  |  |  |

294

295 **4.4 Attributes of glacial lake data**

296 A total of 18 attribute fields were input into our glacial lake datasets (Table 3). They include  
 297 lake location (longitude and latitude), lake elevation (centroid elevation), orbital number of the  
 298 image source, image acquisition date, lake area, lake perimeter, lake types of the two GLCSs,  
 299 mapping uncertainty, lake water volume and the country, sub-basin, and mountain range  
 300 associated with the lake. Amongst the attributes, lake location was calculated based on the

301 centroid of each glacial lake polygon associated with the DEM, N represents northing and E  
302 represents easting. The orbital number of the image source was filled with the corresponding  
303 satellite image, with the codes expressed as “PxxxRxxx” or “Txxxxx”, where P and R indicate  
304 the path and row for Landsat image and T represents the tile of Sentinel-2 image associated  
305 with 5 digit code of military grid reference system. SceneID indicated identifying information  
306 of image source for Landsat or Sentinel-2, consisting of the orbital number, sensor ID, and  
307 acquisition date (YYYYMMDD) for Landsat image, or the orbital number and acquisition date  
308 (YYYYMMDD) for Sentinel-2 image. Area and perimeter were automatically calculated based  
309 on glacial lake extents. Lake water volume was estimated by an area-volume empirical  
310 equation (Cook and Quincey, 2015). Lake types were attributed using the characterization and  
311 interpretation marks described in Section 4.3. Mapping uncertainty was estimated using our  
312 modified equation which will be introduced in section 4.5 and the appendix tutorial. Located  
313 country, sub-basin, and the mountain range of each glacial lake were identified by overlapping  
314 the geographic boundaries of countries, basins, and mountain ranges.

315 **Table 3.** Attributes of glacial lake dataset.

| Field Name      | Type      | Description  | Note   |
|-----------------|-----------|--|--|
| FID or OBJECTID | Object ID | Unique code of glacial lake  | Number   |
| Shape           | Geometry  | Feature type of glacial lake   | Polygon  |
| Latitude        | String    | Latitude of the centroid of glacial lake polygon   | Degree minute second   |
| Longitude       | String    | Longitude of the centroid of glacial lake polygon  | Degree minute second   |
| Elevation       | Double    | Elevation of the centroid of glacial lake polygon  | Unit: meter above sea level  |
| SceneID         | String    | Scene ID of image source for Landsat or Sentinel-2   | PxxxRxxx_xxxYYYYMMDD or Txxxxx_YYYYMMDD  |
| ACQDATE         | String    | The acquisition date of the source image   | YYYYMMDD   |
| GLCS1           | String    | The first classification system of glacial lakes based on the relationship of interaction between glacial lakes and glaciers | Supraglacial, Ice-contact, Unconnected-glacier-fed, and None-glacier-fed                 |
| GLCS2           | String    | The second classification system of glacial lakes is based on lake formation mechanism and dam material properties           | Supraglacial, End-moraine-dammed, Lateral-moraine-dammed, Glacial-erosion and Ice-dammed |
| Basin           | String    | Basin name where the glacial lake locates in   |  |



| Field Name | Type   | Description  | Note               |
|------------|--------|--|--------------------|
| Mountain   | String | Mountain name where the glacial lake locates in  |                    |
| Country    | String | Country name where the glacial lake locates in   |                    |
| Perimeter  | Double | The perimeter of the glacial lake boundary   | Unit: meter        |
| Area       | Double | Area of glacial lake coverage  | Unit: square meter |
| AreaUncer  | Double | Area uncertainty of glacial lake mapping estimated based on modified Hanshaw's equation (2014) | Unit: square meter |
| Operator   | String | The operator of the glacial lake dataset   | Muchu, Lesi        |
| Examiner   | String | Examiner of glacial lake dataset   | Yong, Nie          |
| Volume     | Double | The water volume of a glacial lake estimated by an area-volume empirical equation              | Unit: cubic meter  |

316

## 317 4.5 Error and uncertainty assessment

### 318 4.5.1 Improved uncertainty estimating method

319 We modified Hanshaw's (2014) equation that had been used to calculate lake-area mapping  
320 uncertainty. Lake perimeter and displacement error are widely used to estimate the  
321 uncertainty of glacier and lake mapping from satellite observation (Carrivick and Quincey,  
322 2014; Hanshaw and Bookhagen, 2014; Wang et al., 2020). Hanshaw and Bookhagen (2014)  
323 proposed an equation to calculate the error of area measurement by the number of edge pixels  
324 of the lake boundary multiplied by half of a single pixel area. The number of edge pixels is  
325 simply calculated by the perimeter divided by the grid size. The equation is expressed below:

$$326 \quad \text{Error}(1\sigma) = \frac{P}{G} \times 0.6872 \times \frac{G^2}{2} \quad (2)$$

$$327 \quad D = \frac{\text{Error}(1\sigma)}{A} \times 100\% \quad (3)$$

328 Where  $G$  is the cell size of the remote sensing imagery (10 m for Sentinel-2 image and 30 m  
329 for Landsat image).  $P$  is the perimeter of individual glacial lake (m), and the coefficient of  
330 0.6872 ( $1\sigma$ ), which means nearly 69% of the edge pixels are subject to errors (Hanshaw and  
331 Bookhagen, 2014), was chosen assuming that area measurement errors follow a Gaussian  
332 distribution. Relative error ( $D$ ) was calculated by equation 3, in which  $A$  is the area of an

333 individual glacial lake.

334 In the original equation 2, the number of edge pixels varies by the shape of the lake and is  
 335 indicated by  $\frac{P}{G}$ . However, the pixels in the corner are double-counted (Figure 4). The total  
 336 number of repeatedly calculated edge pixels equals the number of inner nodes. Therefore, we  
 337 adjusted the calculation of the actual number of edge pixels as the maximum of edge pixels  
 338 ( $\frac{P}{G}$ ) subtracting the number of inner nodes. Accordingly, the equation of uncertainty  
 339 estimation for lake mapping is modified as below:

$$340 \quad Error(1\sigma) = \left(\frac{P}{G} - N_{Inner}\right) \times 0.6872 \times \frac{G^2}{2} \quad (4)$$

341 Where  $N_{Inner}$  is the number of inner nodes (inflection points) of each lake. The modified  
 342 equation is also suitable for lakes with islands (as illustrated in Figure 4b).

343 For polygons without islands (Figure 4a), use the following equation:

$$344 \quad N_{Inner} = \left(\frac{N_{Total}-4-1}{2}\right) \quad (5)$$

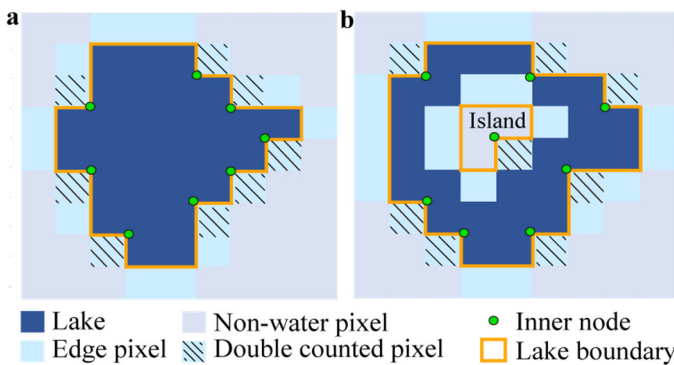
345  $N_{Total}$  is the total number of nodes, including both the outer and inner.  $N_{Total}$  is calculated by  
 346 the ‘‘Field Calculator’’ in ArcGIS, in some cases, it is necessary to remove the redundant  
 347 nodes before calculating the total number of nodes (See the Appendix for more details). An  
 348 inner node is a polygon vertex where the interior angle surrounding it is greater than 180  
 349 degrees. An outer node is the opposite of the inner node, where the interior angle is less than  
 350 180 degrees. We found that the outer nodes are usually four more than the inner nodes in our  
 351 glacial lake dataset. The total nodes in ArcGIS contain one overlapping node to close the  
 352 polygon, meaning the endpoint is also the start point. This extra count was deleted from the  
 353 calculation (equation 5).

354 For polygons with island (Figure 4b) use the following equation:

$$355 \quad N_{Inner} = \left(\frac{N_{Total}-(N_{Island}+1)\times 5}{2}\right) \quad (6)$$

356  $N_{Island}$  is the number of islands within each polygon. A calculation method of  $N_{Island}$  is  
 357 given in the Appendix.

358



361 **Figure 4.** Sketch of estimating the actual edge pixels for uncertainty calculation of individual glacial lakes  
 362 (with (a) and without islands (b)).

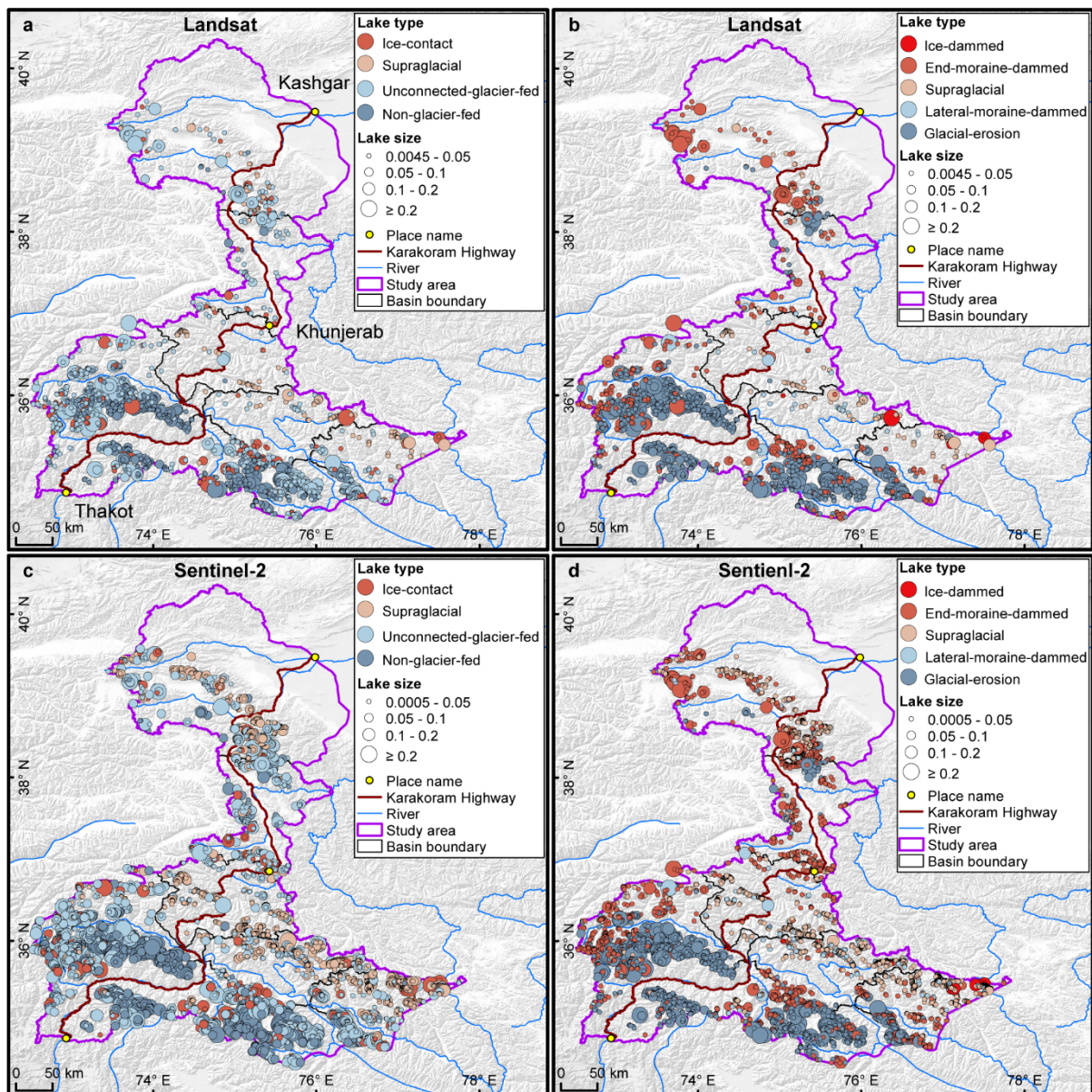
#### 363 4.5.2 Validation of glacial lake mapping

364 A total of 89 glacial lakes were selected by stratified random sampling and manually digitized  
365 based on the Google Earth images in circa 2020 with a spatial resolution of  $\sim 2$  m acquired  
366 from WorldView, GeoEye, Pleiades, etc. satellites to further validate the absolute error of our  
367 glacial lake products in 2020 due to lacking field measurements for glacial lakes in the study  
368 area. During the sampling, we set a minimum lake area to be  $4500 \text{ m}^2$  and a relative  
369 difference between Landsat- and Sentinel-derived lake areas of less than 18% (nearly  
370 equaling the average relative error of  $\pm 17.36\%$  for Landsat lake mapping) to minimize the  
371 effect of lake changes from multi-temporal satellite observations in circa 2020. The 89  
372 sample lakes range from  $0.005 \text{ km}^2$  to  $0.802 \text{ km}^2$  with a median (standard deviation) size of  
373  $0.047 \pm 0.134 \text{ km}^2$  and a total area of  $8.033 \text{ km}^2$  for Landsat-derived dataset, and range from  
374  $0.005 \text{ km}^2$  to  $0.849 \text{ km}^2$  with a median (standard deviation) size of  $0.045 \pm 0.144 \text{ km}^2$  and a  
375 total area of  $8.447 \text{ km}^2$  for Sentinel-derived dataset.  
376

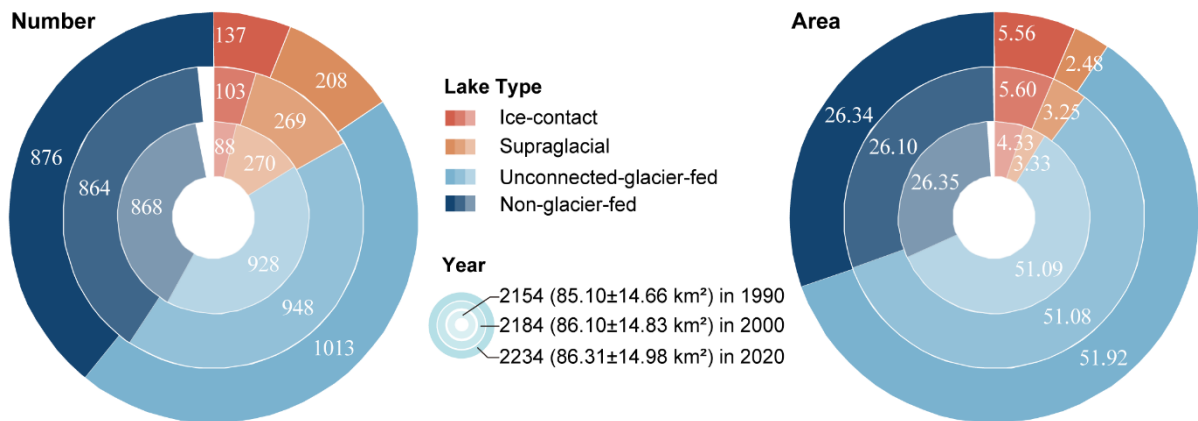
## 377 **5 Results**

### 378 5.1 Glacier lake distribution and changes observed from Landsat

379 We mapped 2,234 glacial lakes for 2020 across the studied CPEC from Landsat-8 images,  
380 with a total area of  $86.31 \pm 14.98 \text{ km}^2$  (Figure 5a and b). Unconnected-glacier-fed lakes are  
381 dominant in the first classification system, followed by non-glacier-fed lakes (Figure 6)  
382 whereas glacial-erosion lakes dominate at both number (1478) and area ( $57.02 \text{ km}^2$ ) in the  
383 second classification system (Figure 7), followed by end-moraine-dammed lakes and  
384 supraglacial lakes. Among the classified lakes, 137 are ice-contact lakes and cover an area of  
385  $5.56 \text{ km}^2$ , implying a higher mean size of ice-contact lakes than supraglacial lakes.  
386

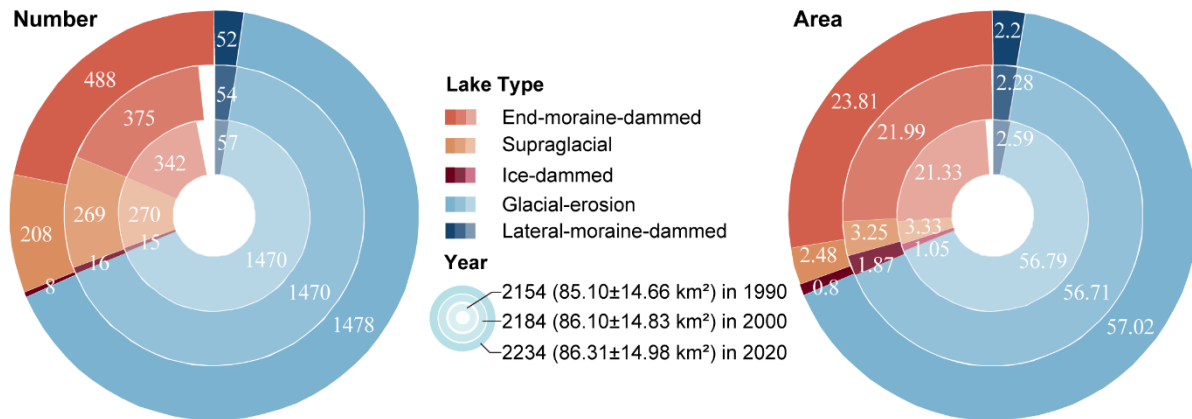


387  
 388 **Figure 5.** Distribution of glacial lakes in 2020 extracted from Landsat (a, b) and Sentinel-2 (c, d) images.  
 389 Panels a and c are classified by GLCS1 and GLCS2 for sub-graph b and d.  
 390



391  
 392 **Figure 6.** The number and area of different types of glacial lakes are classified based on the condition of

393 glacier supply in the study area (GLCS 1). The outermost ring represents glacial lake data in 2020, the  
 394 middle ring for 2000, and the innermost ring for 1990. Lake number and area in 2020 were selected as  
 395 references, meaning a concept of "100 %" for a complete ring. Labeled values are scaled in degrees rather  
 396 than the radius of rings.  
 397



398  
 399 **Figure 7.** The number and area of different types of glacial lakes are classified based on glaciation and the  
 400 nature of the dam in the study area (GLCS 2). The outermost ring represents glacial lake data in 2020, the  
 401 middle ring for 2000, and the innermost ring for 1990. Lake number and area in 2020 were selected as  
 402 references, meaning a concept of "100 %" for a complete ring. Labeled values are scaled in degrees rather  
 403 than the radius of rings.  
 404

405 The total number and area of glacial lakes in the study remain relatively stable with a  
 406 slight increase between 1990 and 2020, and the changes in count and area among various  
 407 types of glacial lakes vary substantially (Figure 6 and Figure 7). From 1990 to 2020, the total  
 408 number of glacial lakes increased by 80 or 3.70%, while the area grew by 1.21 km<sup>2</sup> (or  
 409 1.42%). In GLCS1, unconnected-glacier-fed lakes have the largest increase in number,  
 410 followed by ice-contact and non-glacier-fed lakes, whereas supraglacial lakes decreased by  
 411 62 in count. Ice-contact lakes expanded by 1.24 km<sup>2</sup> (equaling an increase of 26% in ice-  
 412 contact lakes), contributing one-third of the total area increase. Supraglacial lakes decreased  
 413 by 0.85 km<sup>2</sup> in area whereas the areas of unconnected-glacier-fed and non-glacier-fed lakes  
 414 remained stable as a result of disconnections from glaciers (Figure 6). In GLCS2, end-  
 415 moraine-dammed lakes increased by 2.48 km<sup>2</sup> and contributed most of the glacier lake area  
 416 expansion, whereas supraglacial, ice-dammed, and lateral-moraine-dammed lakes decreased  
 417 slightly in both number and area. Glacial-erosion lakes accounted for the maximum  
 418 percentage (about 66% for both count and area) in each period and remained stable (Figure  
 419 7).

## 420 5.2 Glacier lake distribution observed from Sentinel-2

421 Sentinel-derived results show that there are 7,560 glacial lakes (103.70±8.45 km<sup>2</sup>) in 2020  
 422 across the entire CPEC under an MMU of 5 pixels (500 m<sup>2</sup>). Compared with Landsat-derived  
 423 product, glacial lakes from Sentinel-2 have similar spatial distribution characteristics (Figure  
 424 5); meanwhile, a larger quantity of glacier lakes, with more accurate boundaries and a greater  
 425 total lake area, were generated from Sentinel-2 images (Table 4). The smallest size class



426 (0.0005-0.0045 km<sup>2</sup>) contains the maximum lake number (4,969) but the least lake area  
 427 (7.73±2.62 km<sup>2</sup>), which is not available in the Landsat-derived lake data due to a coarser  
 428 spatial resolution. In each size class, the overlap ratios are greater than 85% in count and  
 429 area, and there are also a higher number and larger area of glacial lakes from Sentinel than  
 430 that from Landsat images. Sentinel-2 images (10 m) with a finer spatial resolution produce  
 431 more glacial lakes than those from Landsat images (30 m). The discrepancy is mainly  
 432 attributed to the inconsistency of spatial resolutions and image acquisition dates, as discussed  
 433 in section 6.2.

434

435 **Table 4.** Count and area of glacial lakes mapped from Sentinel-2 and Landsat images in 2020 in various  
 436 size classes.

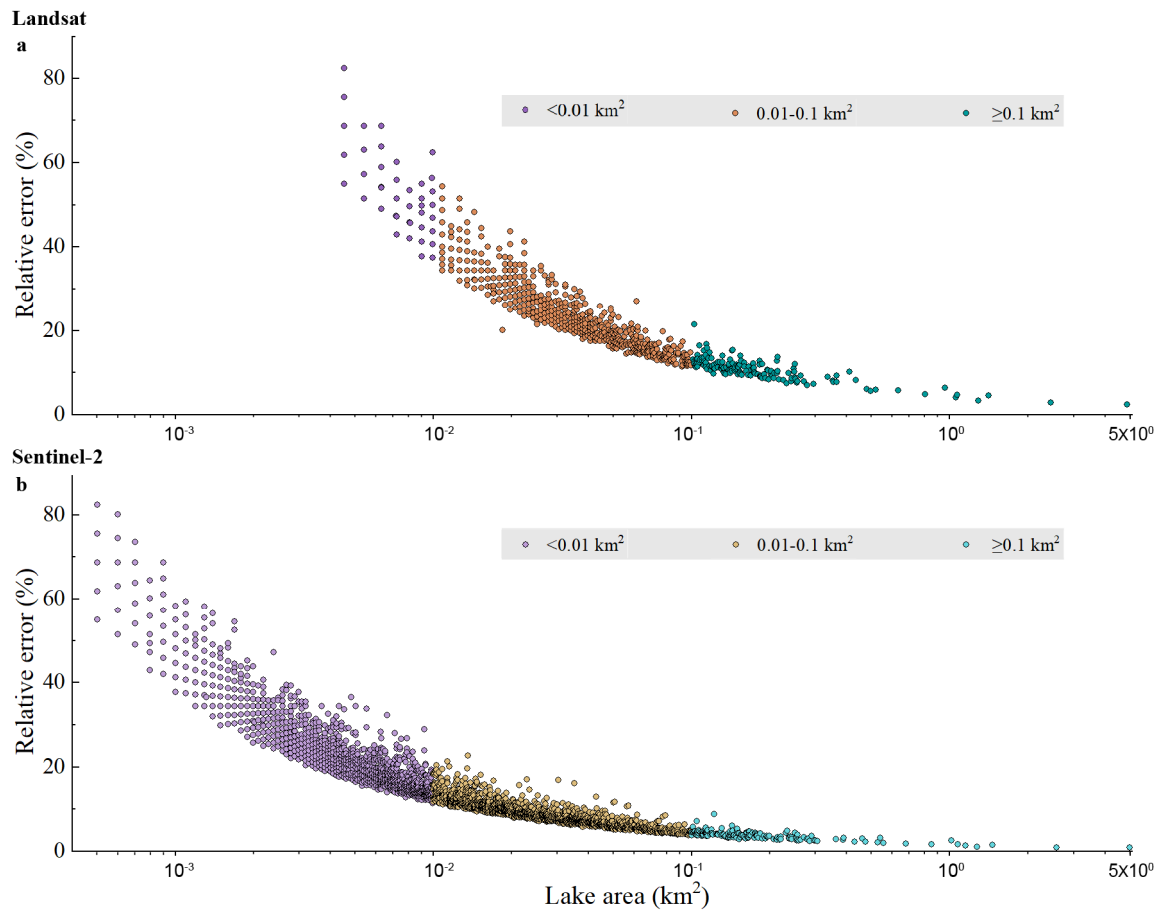
| Lake size<br>km <sup>2</sup> | Glacial lakes from Sentinel-2<br>count (km <sup>2</sup> ) | Glacial lakes from Landsat<br>count (km <sup>2</sup> ) | Overlap<br>% (%) |
|------------------------------|---|--|------------------|
| 0.0045-0.05                  | 2182 (35.52±3.72)   | 1870 (31.47±9.57)                                      | 85.70 (88.60)    |
| 0.05-0.1                     | 237 (16.37±0.89)  | 204 (14.07±2.18)                                       | 86.08 (85.95)    |
| 0.1-0.2                      | 122 (16.88±0.68)  | 115 (15.91±1.83)                                       | 94.26 (94.25)    |
| ≥0.2                         | 50 (27.20±0.54)   | 45 (24.86±1.40)  | 90.00 (91.40)    |
| Total                        | 2591 (95.97±5.83)   | 2234 (86.31±14.98)                                     | 86.22 (89.93)    |

437 Note: Second column excludes 4969 (7.73±2.62 km<sup>2</sup>) lakes in the 0.0005 to 0.0045 km<sup>2</sup> range. Overlap % (%) represents the  
 438 ratios between our Landsat-derived dataset and Sentinel-derived product in count and area, respectively.

## 439 6 Discussions

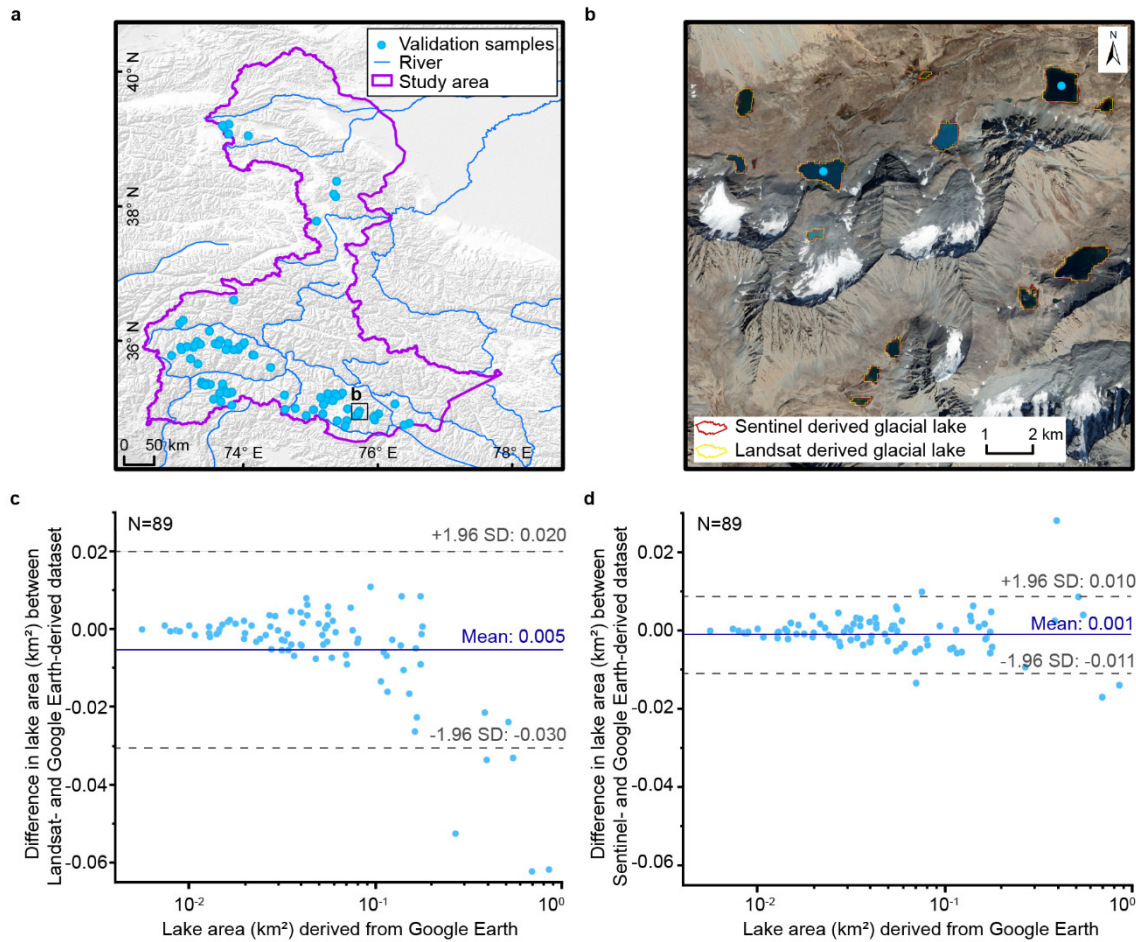
### 440 6.1 Uncertainty and error of lake mapping

441 The uncertainty estimated from our improved equation shows that the relative error of  
 442 individual glacial lakes decreases when lake size increases or the cell size of remote sensing  
 443 images reduces (Lyons et al., 2013; Carrivick and Quincey, 2014) (Figure 8). Total area  
 444 errors of glacial lakes in the study area are approximate ±14.98 km<sup>2</sup> and ±8.45 km<sup>2</sup> in 2020  
 445 for Landsat and Sentinel-2 datasets, respectively, and the average relative errors are ±17.36%  
 446 and ±8.15%. Generally, small lakes have greater relative errors. For example, the mean  
 447 relative error is 35.38% for Landsat-derived glacial lakes between 0.0045 and 0.1 km<sup>2</sup> and  
 448 10.63% for glacial lakes greater than 0.1 km<sup>2</sup>. The mean area error of Sentinel-derived glacial  
 449 lakes is almost one-third of that extracted from Landsat images for glacial lakes of all or  
 450 specific size groups. Because the relative error was estimated as a function of satellite image  
 451 spatial resolution and lake perimeter, the calculated error for a large lake is proportionally  
 452 smaller than that of a small lake (Salerno et al., 2012) and the error for Landsat-derived lake  
 453 is naturally greater than that of Sentinel-derived lake at the same size group.



454  
 455 **Figure 8.** The estimated relative error for glacial lakes of all or specific size ranges in the study area. Error  
 456 estimation is based on the modified equation and lake data extracted from Landsat (a) and Sentinel-2  
 457 images (b).

458  
 459 Our Landsat- and Sentinel-derived glacial lake dataset match well lake boundaries in Google  
 460 Earth higher resolution images (Figure 9). The mean difference in area is 0.005 km<sup>2</sup> between  
 461 Landsat- and Google Earth-derived lakes and 0.001 km<sup>2</sup> between Sentinel- and Google Earth-  
 462 derived lakes, and major validation samples (84/89) are within the confidence interval of  
 463 95%, indicating high accuracy in lake mapping (Figure 9c and d). The error of 89 sample  
 464 lakes is 5.48% in the total area between Landsat- and Google Earth-derived data, and 0.61%  
 465 for Sentinel- and Google Earth-derived data. The median ( $\pm$ standard deviation) in a  
 466 discrepancy of the individual lake area is 7.66 $\pm$ 4.96 % for Landsat- and Google Earth-derived  
 467 data, and 4.46 $\pm$ 4.62 % for Sentinel- and Google Earth-derived data. Our glacial lake dataset  
 468 shows satisfactory mapping accuracy, although Sentinel-derived lake data performs more  
 469 accurately than those from Landsat images. We also validated the sampling of Landsat-  
 470 derived 89 lakes by the existing Landsat-extracted lake data produced by Wang et al. (2020).  
 471 A total of 83 lakes are available in Wang’s data with a mean difference of 0.005 km<sup>2</sup> in the  
 472 lake area (Figure A8). This also shows an improvement in our lake product in contrast to the  
 473 existing dataset.



474

475

476

477

478

**Figure 9.** Distribution of the validation sample (a), visual comparison of glacial lakes derived from Landsat and Sentinel-2 images overlaying Google Earth imagery (© Google Earth 2019) in a zoomed site (b), and differences between our glacial lake product (mapped from Landsat and Sentinel-2 images) and the validation reference (digitized from Google Earth images) (c and d).

479

## 6.2 Comparison of Sentinel- and Landsat-derived products

480

481

482

483

484

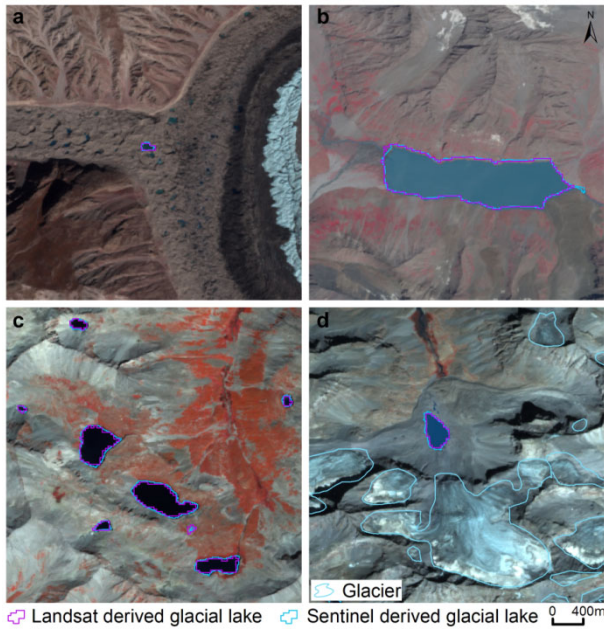
485

486

487

Glacial lakes from Landsat and Sentinel-2 images have high consistency in number and area with overlap rates from approximately 86% to 94% for all lakes greater than 0.0045 km<sup>2</sup> (Table 4), indicating a good potential for coordinated utility with Landsat archived observation (Figure 10). Lake extents extracted from Landsat and Sentinel images match well for various types and sizes (Figure 10 and Figure 11, Table 4). The best consistency rate reaches 94% for the glacial lakes between 0.1 km<sup>2</sup> and 0.2 km<sup>2</sup>. The difference in the area of glacial lakes extracted from Landsat and Sentinel-2 images generally lies within the uncertainty ranges.





488

489 **Figure 10.** High consistency of lake extents extracted from Landsat and Sentinel-2 images. Lake types  
 490 shown include supraglacial (a), glacier-fed moraine-dammed (b), unconnected glacial-erosion lake without  
 491 glacier melt supply (c), and glacier-fed moraine-dammed lakes (d).

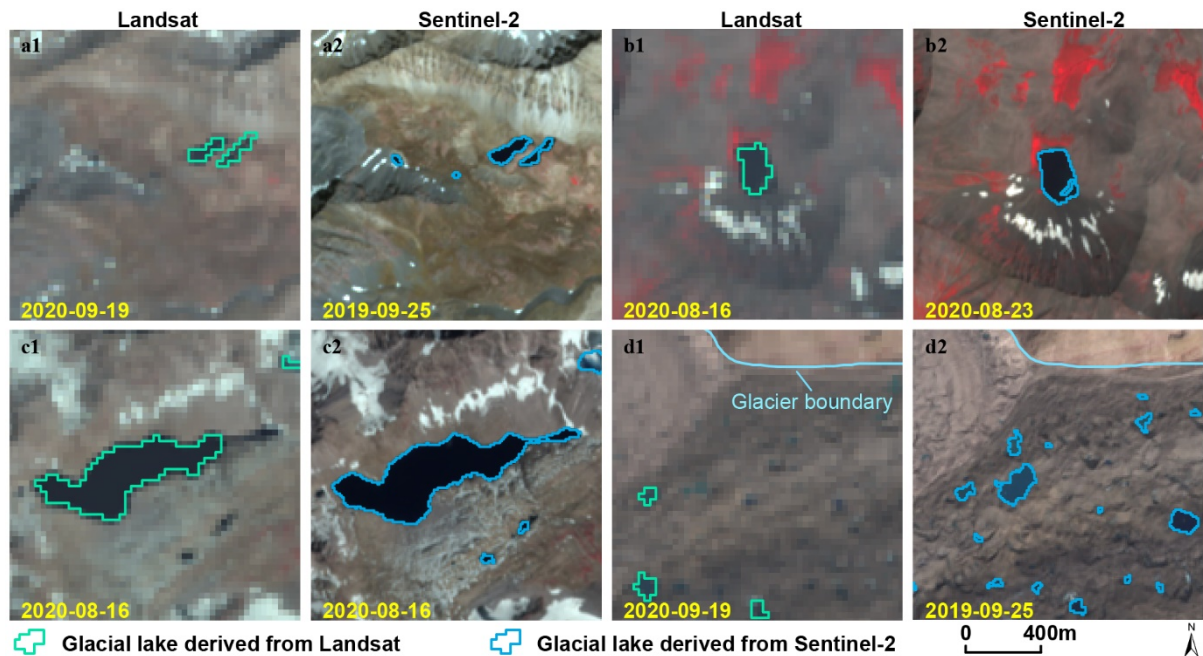
492

493 The spatial resolution of satellite images plays a primary role in the discrepancies in count  
 494 and area of glacial lakes extracted from Landsat (30 m) and Sentinel-2 (10 m) observations.  
 495 Due to a finer spatial resolution, Sentinel-2 images can extract more glacial lakes and more  
 496 accurate extents than those from Landsat images. We set the same 5 pixels as the MMU for  
 497 both Landsat and Sentinel-2 images, which corresponds to a minimum area of  $0.0045 \text{ km}^2$   
 498 and  $0.0005 \text{ km}^2$ , respectively. The minimum mapping area results in generating nearly 5000  
 499 more lakes from Sentinel-2 images than from Landsat images, causing the greatest  
 500 discrepancy in number, such as Figure 11. Small lakes such as supraglacial lakes play an  
 501 important role in analyzing glacier evolution and supraglacial drainage systems (Liu and  
 502 Mayer, 2015; Miles et al., 2018), implying a potential of our dataset to be applied in studies  
 503 of glacier-lake evolutions. Meanwhile, Sentinel-2 images can depict boundaries of glacial  
 504 lakes with lower uncertainty, as some small islands and narrow channels (Figure 11b and c)  
 505 were mapped from Sentinel-2 imagery that was unable to be detected in Landsat imagery.

506

507 In addition to the difference in image resolution, different acquisition dates between  
 508 Sentinel-2 and Landsat images can also contribute to the discrepancy between those two  
 509 glacial lake datasets. The total number of supraglacial lakes and ice-dammed glacial lakes are  
 510 less than 300, but those lakes are controlled by glacier movement and temperature changes  
 511 (Liu and Mayer, 2015; Miles et al., 2018), which vary faster with time than relatively stable  
 512 glacial-erosion and moraine-dammed lakes. Acquiring same-day images from the two sensors  
 513 was not always possible due to the impacts of cloud contaminations, topographic shadows,  
 514 snow cover, and revisit periods (Williamson et al., 2018; Paul et al., 2020). Despite our  
 515 efforts of leveraging all available high-quality images, the overlap of acquisition dates  
 516 between Landsat and Sentinel-2 images for the same location is relatively low (only 7 scenes  
 of Sentinel-2 images or 112 glacial lakes in 2020) in this study area, and the consequential

517 temporal gaps led to a difference in the number and area of the derived glacial lakes. As  
 518 exemplified in Figure 11d, the mapped supraglacial lakes in the same location exhibit a  
 519 considerable discrepancy, which is likely a joint consequence of both sensor difference and  
 520 glacier lake evolution.  
 521



522 **Figure 11.** The discrepancy of lake extents extracted from Landsat and Sentinel-2 images.  
 523  
 524

525 **6.3 Comparison with the previous similar dataset**

526 An increasing number of glacier lake datasets have been released over the past years, and  
 527 most of them were produced from long-term Landsat archives. Regional glacial lake datasets  
 528 using Sentinel images are scarce. The lack of Sentinel-derived glacial lake data in the study  
 529 area makes it impossible to compare. Here we selected four available glacial lake datasets to  
 530 compare with our Landsat-derived dataset at the same MMU and study area.

531 We provide the latest glacial lake dataset (in 2020) and the most long-term 30-m Landsat  
 532 observation (1990 to 2020) for this study, with a range of critical attributes including two  
 533 types of classification systems. Within the same study area, our 2020 glacial lakes appear to  
 534 be closest to the 2018 dataset produced by Wang et al. (2020), with the highest overlap of  
 535 greater than 91% in count at the minimum mapping unit of 5400 m<sup>2</sup> or 6 pixels (Table 5).  
 536 Wang’s dataset (2020) contains many large landslide-dammed lakes that are excluded in our  
 537 glacial lake mapping, so their total glacier lake area is greater than ours. The overlapping  
 538 rates between Wang’s glacial lakes (2020) in 1990 and ours are more than 83% in count.  
 539 However, their results show a distinct increase of glacial lakes in number and area between  
 540 1990 and 2018 (Wang et al., 2020) whereas our data show a more stable change between  
 541 1990 and 2020. One possible reason is that manually delineating glacial lakes twice by  
 542 different operators during Wang’s lake mapping (2020) exacerbates the errors of mapping.  
 543 Another reason is that their data contains landslide-dammed lakes that fluctuate greatly with  
 544 time and expanded recently. One example is Attabad Lake (Located at 36°18'22.33"N,

545 74°49'34.36"E).

546

547 **Table 5.** Comparison between our Landsat-based mapping and other third-party Landsat-based glacial lake  
548 datasets in the study area.

| Baseline year<br>(them/us) | Method<br>(them/us)               | MMU<br>m <sup>2</sup> (pixels) | Count<br>(them) | Count<br>(us) | Ratio<br>(%) | Reference           |
|----------------------------|-----------------------------------|--------------------------------|-----------------|---------------|--------------|---------------------|
| 1990/1990                  | Manual/Semi-automated             | 5400 (6)                       | 1720            | 2069          | 83.13        | Wang et al., 2020   |
| 1990/1990                  | Automated/Semi-automated          | 50000 (55)                     | 145             | 363           | 39.94        | Shugar et al., 2020 |
| 1990/1990                  | Manual/Semi-automated             | 4500 (5)*                      | 622             | 2154          | 28.88        | Zhang et al., 2015  |
| 2000/2000                  | Manual/Semi-automated             | 4500 (5)*                      | 724             | 2184          | 33.15        | Zhang et al., 2015  |
| 2000/2000                  | Automated/Semi-automated          | 50000 (55)                     | 155             | 361           | 42.94        | Shugar et al., 2020 |
| 2008/2000                  | Automated & Manual/Semi-automated | 8100 (9)                       | 1067            | 1800          | 59.28        | Chen et al., 2021   |
| 2015/2020                  | Automated/Semi-automated          | 50000 (55)                     | 148             | 364           | 40.66        | Shugar et al., 2020 |
| 2017/2020                  | Automated & Manual/Semi-automated | 8100 (9)                       | 1063            | 1813          | 58.63        | Chen et al., 2021   |
| 2018/2020                  | Manual/Semi-automated             | 5400 (6)                       | 1956            | 2149          | 91.02        | Wang et al., 2020   |

549 Note: MMU represents the minimum mapping unit that is possible to enable a valid comparison between our product and each  
550 of the third-party datasets. \* The MMU in the dataset of Zhang et al. (2015) is 3 pixels, finer than 5 pixels in our product, so  
551 an MMU threshold of 5 pixels was used for this comparison.

552

553 The second highest overlapping rate is approximate 59% for 2008 and 58% for 2017 in  
554 count comparing with Chen's data (Chen et al., 2021). Similarly, the overlapping rate between  
555 Shugar's dataset (2020) and ours is lower than 43% in count at the minimum mapping unit of  
556 50000 m<sup>2</sup>. The dataset from Zhang et al. (2015) shows fewer glacial lakes in 1990 and 2000 at  
557 the same MMU of 5 pixels. Our product has more lakes than each of the other 4 products at 9  
558 time periods. By inspecting their dataset, we attributed this anomalous discrepancy to a range  
559 of glacial lakes that were missing due to a lack of thorough cross-check quality assurance  
560 during their lake mapping over a larger study area. And those more glacial lakes show an  
561 improvement of our product in contrast to the previous similar datasets. Our Landsat-derived  
562 glacial lake dataset has been visually cross-checked over three time periods after the step of  
563 threshold-based semi-automated lake mapping and has also been visually validated by  
564 Sentinel-derived glacial lakes. Through this series of quality assurance, we aim at delivering  
565 one of the most reliable multi-decadal glacial lake products for this study area.

566 Other factors, such as image quality and acquisition dates, mapping methods, and quality  
567 assurance workflow, might also lead to discrepancies between the glacial lake datasets. Despite  
568 such discrepancies, an increasing number of publically-shared datasets benefit potential users  
569 to select the most suitable one for their objectives. Herein, we provide an up-to-date glacial  
570 lake dataset derived from both Landsat and Sentinel-2 observations, which further increased  
571 the availability of glacial lake dataset for water resource and GLOFs risk assessment, predicting  
572 glacier-lake evolutions (Carrivick et al., 2020) in the context of climate change.

573

#### 574 6.4 Limitation and updating plan

575 We would like to acknowledge several limitations of our glacier lake dataset, largely due to  
576 the availability of high-quality satellite images in the study area and inadequate field survey  
577 data (Wang et al., 2020; Chen et al., 2021). First, it is unlikely to collect enough good-quality  
578 images within one calendar year for the entire study area due to the high possibility of cloud

579 or snow cover. Even though the capacity of repeat observations for Landsat-8 OLI and  
580 Sentinel-2 increased (Roy et al., 2014; Williamson et al., 2018; Wulder et al., 2019; Paul et  
581 al., 2020), the 2020 glacial lake dataset has to employ images acquired in adjacent years  
582 besides 2020. Most images used from Landsat and Sentinel-2 platforms were imaged in  
583 autumn, and some images taken between April and July and in November also were  
584 employed. Distribution and changes in glacial lakes primarily represent the characteristics  
585 between August and October. Glacial lakes evolve with time and space (Nie et al., 2017), and  
586 subtle inter- and intra-annual changes (Liu et al., 2020) for each period were ignored. Second,  
587 field investigation data are limited due to the low accessibility of the high mountain  
588 environment in the study area, which restrained the accuracy in classifying the glacial lake  
589 types. Although very high-resolution Google Earth images were utilized to assist in lake-type  
590 interpretation, occasional misclassification was unavoidable. We implemented two types of  
591 classification systems based on a careful utilization of glacier data, DEM, geomorphological  
592 features, and expert knowledge. However, the lack of in situ surveys prohibited a thorough  
593 validation of the glacial lake types. Third, the rigorous quality assurance and cross-check  
594 after semi-automated lake mapping assures the quality of our lake dataset but are still time  
595 and cost-prohibitive. State-of-the-art mapping methods, such as deep learning method (Wu et  
596 al., 2020), Google Earth Engine cloud-computing (Chen et al., 2021), and synergy of SAR  
597 and optical images (Wangchuk and Bolch, 2020; How et al., 2021), would be used in the  
598 future to balance product accuracy and time cost.

599 The glacial lake dataset will be updated using newly collected Landsat and Sentinel  
600 images at a five-year interval or modified according to user feedback. The updated glacial  
601 lake dataset will continue to be released freely and publicly on the Mountain Science Data  
602 Center sharing platform.

## 603 **7 Data availability**

604 Our glacial lake dataset extracted from Sentinel-2 images in 2020 and Landsat observation  
605 between 1990 and 2020 are available online via the Mountain Science Data Center, the  
606 Institute of Mountain Hazards and Environment, the Chinese Academy of Sciences at  
607 <https://doi.org/10.12380/Glaci.msdc.000001> (Lesi et al., 2022). The glacial lake dataset is  
608 provided in both ESRI shapefile format (total size of 22.6 MB) and the Geopackage format  
609 (version 1.2.1) with a total size of 9.2MB, which can be opened and further processed by  
610 open-source geographic information system software such as QGIS.

## 611 **8 Conclusions**

612 Glacial lake inventories of the entire China-Pakistan Economic Corridor in 2020 were  
613 provided based on Landsat and Sentinel-2 images using a threshold-based semi-automated  
614 mapping method. Both Landsat and Sentinel-2 derived glacial lake dataset show similar  
615 characteristics in spatial distribution and the statistics of count and area. By contrast, the  
616 glacial lake dataset derived from Sentinel-2 images with a spatial resolution of 10 m has a  
617 lower mapping error and more accurate lake boundary than those from 30 m spatial  
618 resolution Landsat images whereas Landsat imagery is more suitable to analyze spatial-  
619 temporal changes at a longer time scale due to its long-term archived observations at a

620 consistent 30 m spatial resolution starting from the late 1980s.

621 Glacial lakes in the study area remain relatively stable with a slight increase in number and  
622 area between 1990 and 2020 according to Landsat observations. Our dataset reveals that 2154  
623 glacial lakes in 1990 covering  $85.1 \pm 14.66 \text{ km}^2$  increased to 2234 lakes with a total area of  
624  $86.31 \pm 14.98 \text{ km}^2$ . The same mapping method and rigorous workflow of quality assurance  
625 and quality control used in this study reduced the error in multi-temporal changes of glacial  
626 lakes.

627 Hanshaw's error estimation method for pixel-based lake mapping was improved by  
628 removing repeatedly calculated edge pixels that vary with lake shape. Therefore, the newly  
629 proposed method reduces the estimated value of uncertainty from satellite observations. The  
630 average relative error is  $\pm 17.36\%$  for the Landsat-derived dataset and  $\pm 8.15\%$  for the product  
631 from Sentinel-2.

632 Our glacial lake dataset contains a range of critical parameters that maximize their  
633 potential utility for water resource and GLOFs risk evaluation, cryosphere-hydrological, and  
634 glacier-lake evolution projection. The dual classification systems of glacial lake types were  
635 developed and are very likely to attract broader researchers and scientists to use our datasets.  
636 In comparison with other existing glacial lake datasets, our products were created through a  
637 thorough consideration of lake types, cross-checks, and rigorous quality assurance, and will  
638 be updated and released continuously in the Mountain Science Data Center. As such, we  
639 expect that our glacial lake dataset will have significant value to cryospheric-hydrology  
640 research, the assessment of water resources, and glacier-related hazards in the CPEC.

641

642 **Appendix.** The appendix related to this article is available online.

643

644 **Author contributions.** ML and YN conceived the study, ML, YN and XD performed data  
645 processing and analysis of the glacial lake inventory data, JW contributed to tool  
646 development and mapping methods, and ML and YN wrote the manuscript. All authors  
647 reviewed and edited the manuscript before submission.

648

649 **Competing interests.** The authors declare no conflict of interest.

650

651 **Acknowledgments.**

652 We are grateful to the chief editor (ice) Kenneth Mankoff and three anonymous referees for  
653 their constructive comments that greatly help us to improve this manuscript. This study was  
654 supported by the second Tibetan Plateau Scientific Expedition and Research Program (grant  
655 2019QZKK0603), the National Natural Science Foundation of China (Grant Nos. 42171086,  
656 41971153), the International Science & Technology Cooperation Program of China (No.  
657 2018YFE0100100), the Chinese Academy of Sciences "Light of West China" and Natural  
658 Sciences and Engineering Research Council of Canada (Grant No. DG-2020-04207).

659

660

661 **Appendix**

662 **Tutorial for Improved Uncertainty Estimating Method**

663  
664 Hanshaw’s equation was originally proposed for pixelated polygons (such as a polygon  
665 directly extracted from a remote sensing image), and performed more robustly than manually  
666 digitized polygons (where vertices do not necessarily follow the pixel edges). Our improved  
667 method also performs better for pixelated polygons. This tutorial is dedicated to helping  
668 implement our improved uncertainty estimation method.

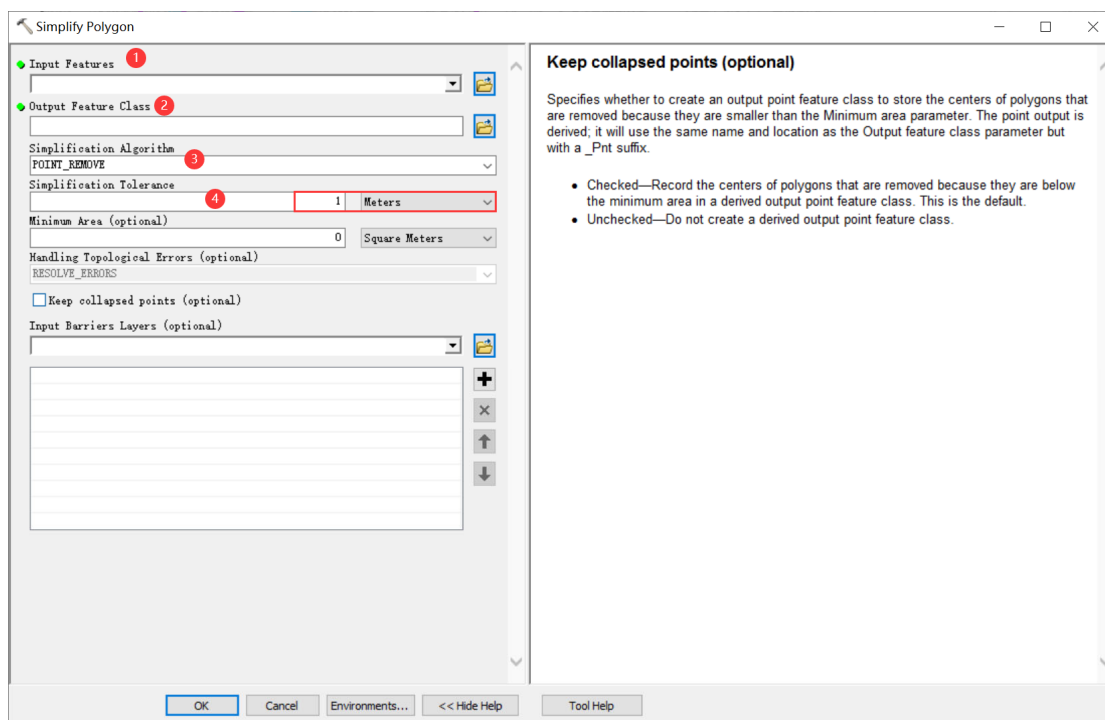
669  
670 **The procedure of uncertainty estimating method (using ArcGIS (© ESRI) for example)**

671 1. Removing redundant nodes (optional)

672 We found that a small proportion (~1%) of the pixelated lake polygons (directly extracted  
673 from satellite images) have redundant nodes, which affects the value of inner nodes. If no  
674 redundant nodes exist, this step can be skipped. Or, we recommend using the “Simplify  
675 Polygon” tool in ArcGIS to remove those nodes (Figure A1).

676 In the Simplify Polygon panel

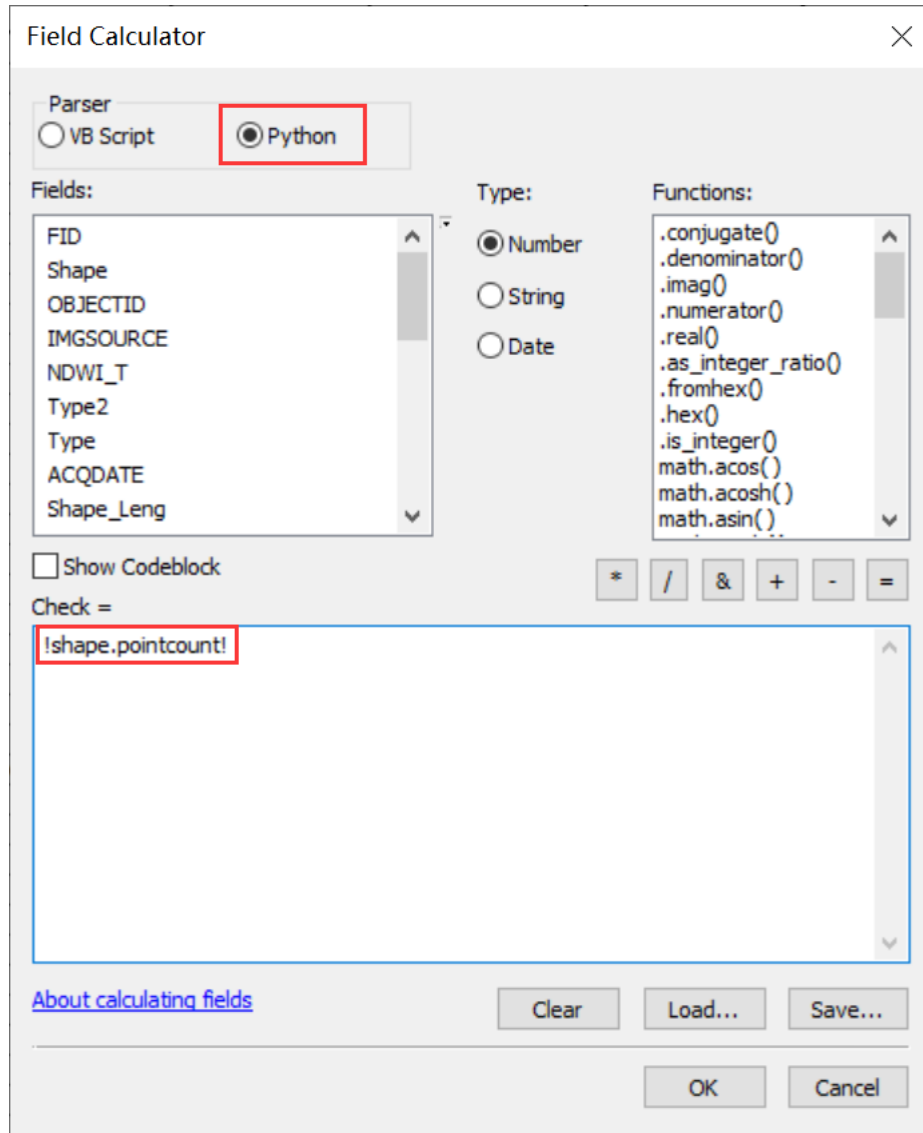
- 677
- 678 • Input your dataset.
  - 679 • Set the output path and output file name.
  - 680 • Choose the simplification algorithm. We recommended “POINT\_REMOVE”.
  - 681 • Set the tolerance of the simplification algorithm. In this step, we need to ensure that the  
682 polygon boundaries remain unchanged after deleting redundant nodes. Generally, a  
tolerance of 1 meter will suffice, or you can adjust the threshold until your satisfaction.



683  
684 **Figure A1.** Input and option for Simplify Polygon in ArcGIS.  
685



- 686 2. Calculating the total number of nodes using ArcGIS (Figure A2):
- 687 • Add a new field in the attribute table of the dataset.
- 688 • Open Field Calculator.
- 689 • Switch the parser to python-mode, and enter the following code “!shape.pointcount!” in
- 690 the blue box to calculate the total number of nodes for each glacial lake boundary.



691

692 **Figure A2.** Total node calculation in ArcGIS.

693

694 3. Calculating the number of inner nodes:

695

696 For polygons without islands (Figure A3), use equation 5. An inner node is a polygon vertex

697 where the interior angle surrounding it is greater than 180 degrees. An outer node is the

698 opposite of the inner node, where the interior angle is less than 180 degrees. We found that

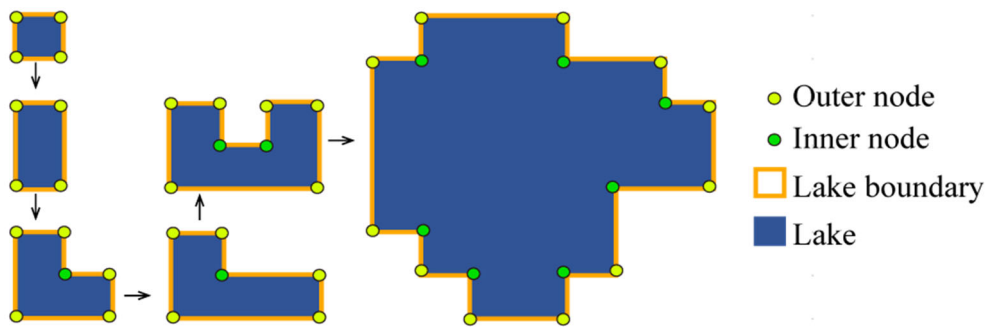
699 the outer nodes are usually four more than the inner nodes in our glacial lake dataset. The

700 total nodes in ArcGIS contain one overlapping node to close the polygon, meaning the

701 endpoint is also the start point. This extra count was deleted from the calculation (equation

702 5).

703



704

705

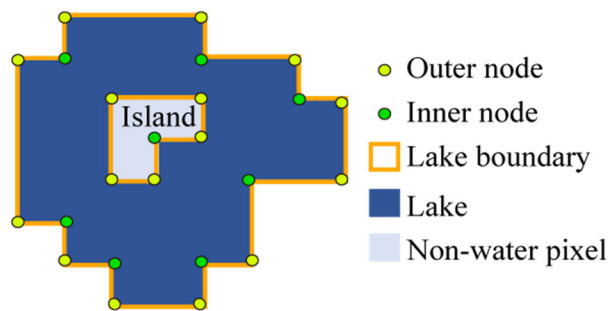
706

707

708

**Figure A3.** Sketch of outer and inner nodes of various glacial lakes without island.

For polygons with islands (Figure A4) use equation 6.



709

710

711

712

713

714

715

716

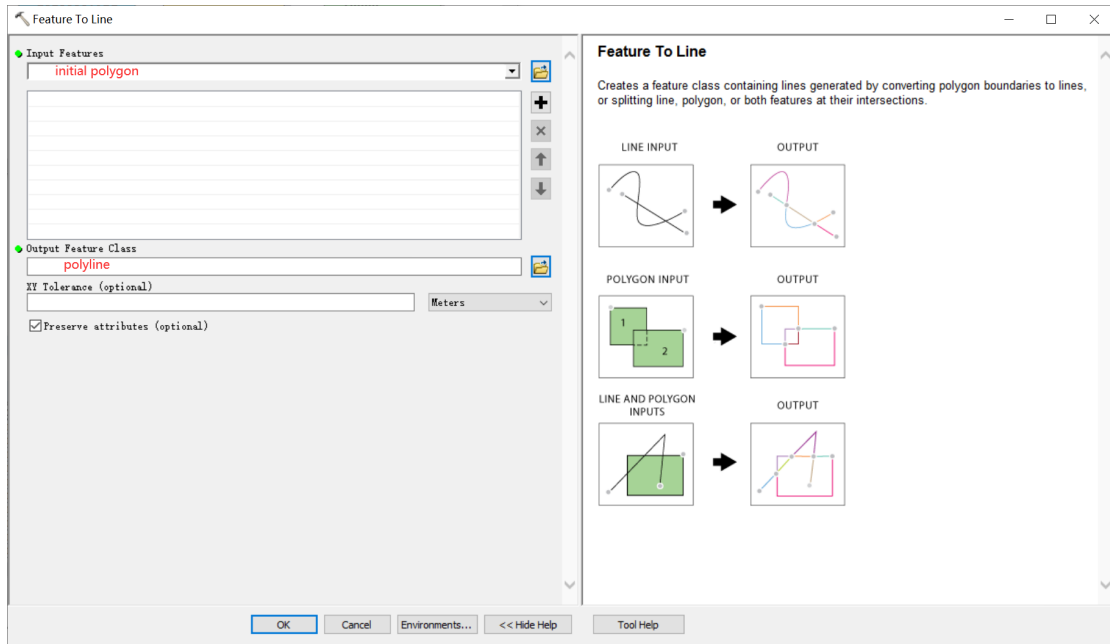
**Figure A4.** Sketch of outer and inner nodes for a glacial lake with an island.

We further specify the steps below to help implement equation 6.

Sept 1: detect the number of islands within each polygon.

- Convert the initial lake polygon to a polyline using the “Feature To Line” tool (Figure A5).

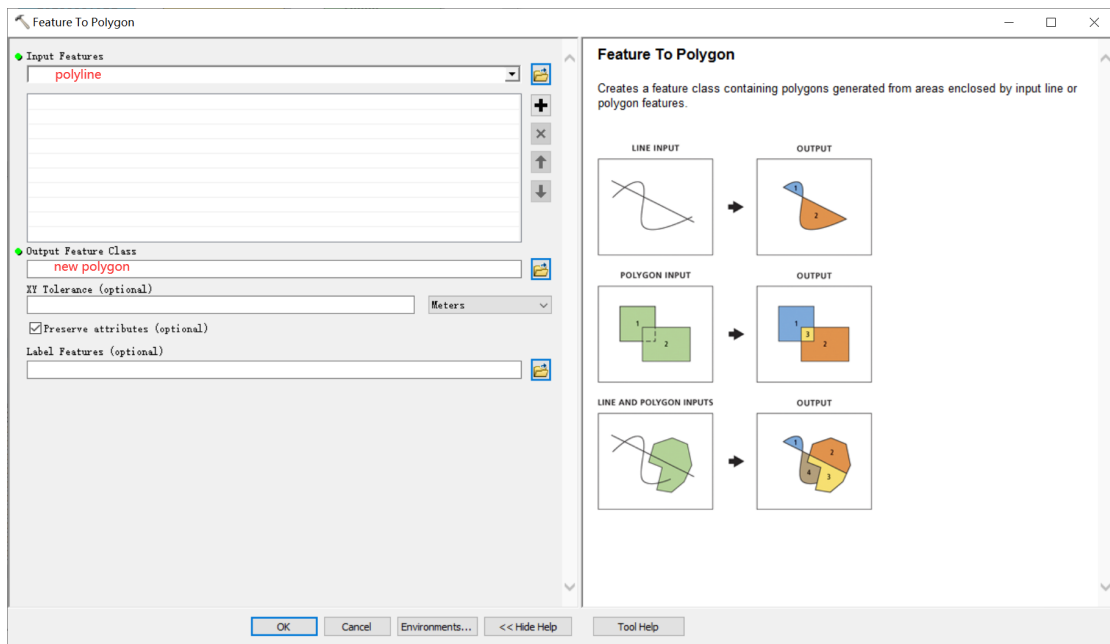




717  
718  
719  
720

**Figure A5.** Feature To Line tool in ArcGIS

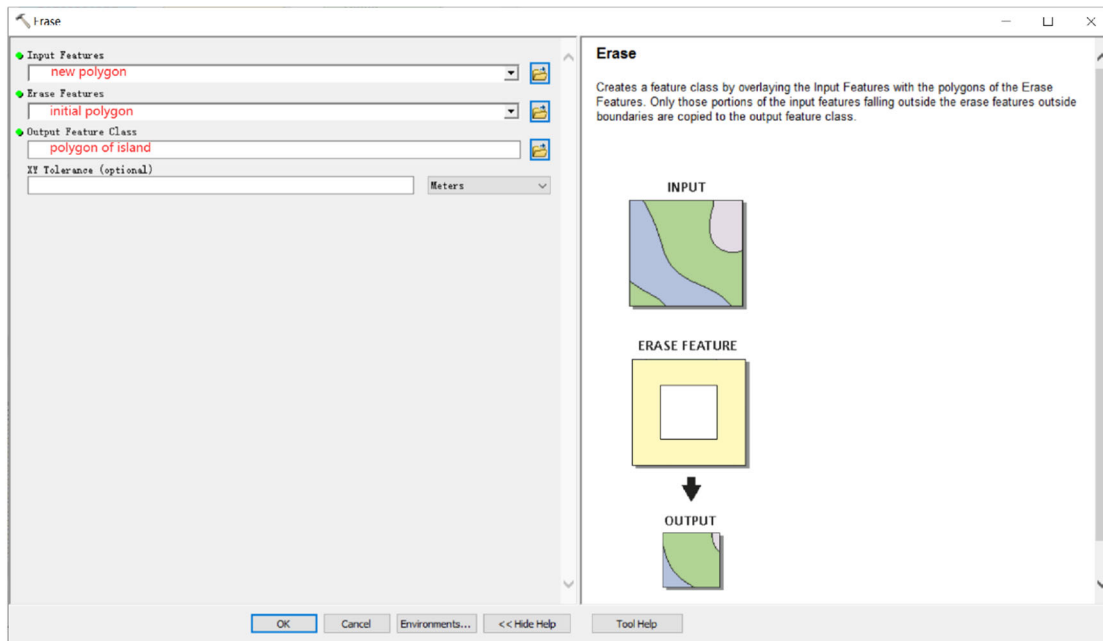
- Convert the polyline to generate a new polygon (Figure A6).



721  
722  
723  
724  
725

**Figure A6.** Feature To Polygon tool in ArcGIS

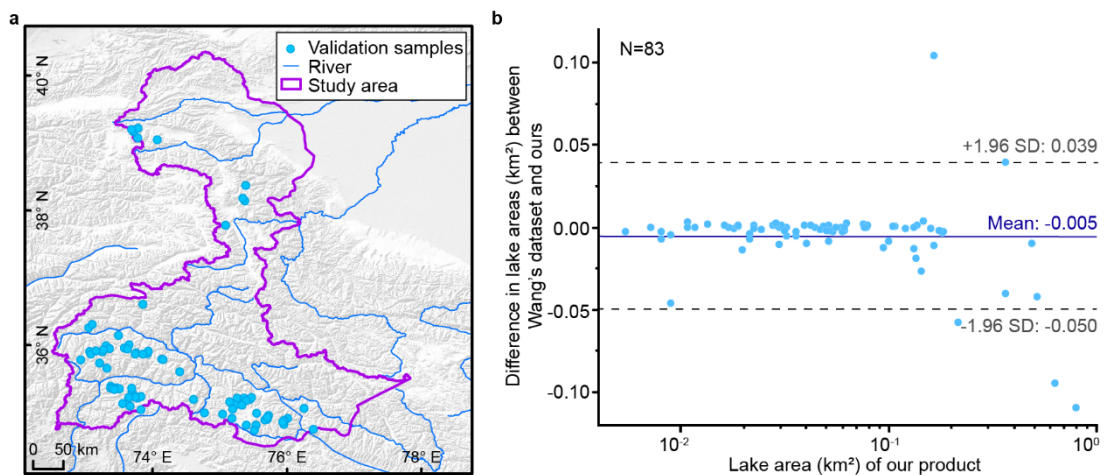
- Erase the new polygon by the initial polygon, which outputs the islands. Then we can count how many islands there are in each lake (Figure A7).



726  
727 **Figure A7.** Erase tool in ArcGIS.  
728

729 Step 2: calculate the number of inner nodes for each polygon with an island or islands using  
730 equation 6.

731  
732 4. Calculating the uncertainty of lake mapping using equation 4.  
733  
734



735  
736 **Figure A8.** Distribution of validation samples (a) and comparison of glacial lakes (b) derived from our  
737 Landsat product in 2020 and Wang's lake data in 2018.  
738

## 739 **References:**

- 740 [1]. Lesi, M., et al., Landsat and Sentinel-derived glacial lake dataset in the China-Pakistan Economic Corridor  
741 from 1990 to 2020. Mountain Science Data Center, 2022.  
742 [2]. Wang, X., S. Liu and J. Zhang, A new look at roles of the cryosphere in sustainable development. Advances

743 in *Climate Change Research*, 2019. 10(2): p. 124-131.

744 [3]. Viviroli, D., et al., Increasing dependence of lowland populations on mountain water resources. *Nature*

745 *Sustainability*, 2020. 3(11): p. 917-928.

746 [4]. Pritchard, H.D., Asia's shrinking glaciers protect large populations from drought stress. *Nature*, 2019.

747 569(7758): p. 649-654.

748 [5]. Nie, Y., et al., Glacial change and hydrological implications in the Himalaya and Karakoram. *Nature*

749 *Reviews Earth & Environment*, 2021. 2(2): p. 91-106.

750 [6]. Brun, F., et al., A spatially resolved estimate of High Mountain Asia glacier mass balances from 2000 to

751 2016. *Nature Geoscience*, 2017. 10(9): p. 668-673.

752 [7]. Shean, D.E., et al., A Systematic, Regional Assessment of High Mountain Asia Glacier Mass Balance.

753 *Frontiers in Earth Science*, 2020. 7: p. 363.

754 [8]. Bhattacharya, A., et al., High Mountain Asian glacier response to climate revealed by multi-temporal satellite

755 observations since the 1960s. *Nature Communications*, 2021. 12(1): p. 4133.

756 [9]. Maurer, J.M., et al., Acceleration of ice loss across the Himalayas over the past 40 years. *Science Advances*,

757 2019. 5(6): p. eaav7266.

758 [10]. Huss, M. and R. Hock, Global-scale hydrological response to future glacier mass loss. *Nature Climate*

759 *Change*, 2018. 8(2): p. 135-140.

760 [11]. Carrivick, J.L. and F.S. Tweed, A global assessment of the societal impacts of glacier outburst floods. *Global*

761 *and Planetary Change*, 2016. 144: p. 1-16.

762 [12]. Nie, Y., et al., An inventory of historical glacial lake outburst floods in the Himalayas based on remote

763 sensing observations and geomorphological analysis. *Geomorphology*, 2018. 308: p. 91-106.

764 [13]. Zheng, G., et al., Increasing risk of glacial lake outburst floods from future Third Pole deglaciation. *Nature*

765 *Climate Change*, 2021. 11(5): p. 411-417.

766 [14]. Rounce, D.R., R. Hock and D.E. Shean, Glacier Mass Change in High Mountain Asia Through 2100 Using

767 the Open-Source Python Glacier Evolution Model (PyGEM). *Frontiers in Earth Science*, 2020. 7: p. 331.

768 [15]. Shugar, D.H., et al., A massive rock and ice avalanche caused the 2021 disaster at Chamoli, Indian Himalaya.

769 *Science*, 2021. 373(6552): p. 300-306.

770 [16]. Shugar, D.H., et al., Rapid worldwide growth of glacial lakes since 1990. *Nature Climate Change*, 2020.

771 10(10): p. 939-945.

772 [17]. Immerzeel, W.W., et al., Importance and vulnerability of the world's water towers. *Nature*, 2020.

773 577(7790): p. 364-369.

774 [18]. Carrivick, J.L., et al., Ice-Marginal Proglacial Lakes Across Greenland: Present Status and a Possible Future.

775 *Geophysical Research Letters*, 2022. 49(12): p. e2022GL099276.

776 [19]. Li, Z., X. Deng and Y. Zhang, Evaluation and convergence analysis of socio-economic vulnerability to

777 natural hazards of Belt and Road Initiative countries. *Journal of Cleaner Production*, 2021. 282(125406): p.

778 125406.

779 [20]. Battamo, A.Y., et al., Mapping socio-ecological resilience along the seven economic corridors of the Belt

780 and Road Initiative. *Journal of Cleaner Production*, 2021. 309(127341): p. 127341.

781 [21]. Hewitt, K., *Glaciers of the Karakoram Himalaya: Glacial Environments, Processes, Hazards and Resources*.

782 2014, Dordrecht: Springer.

783 [22]. Bhambri, R., et al., Ice-dams, outburst floods, and movement heterogeneity of glaciers, Karakoram. *Global*

784 *and Planetary Change*, 2019. 180(9): p. 100-116.

785 [23]. Wang, X., et al., Glacial lake inventory of high-mountain Asia in 1990 and 2018 derived from Landsat

786 images. *Earth System Science Data*, 2020. 12(3): p. 2169-2182.

787 [24]. Nie, Y., et al., A regional-scale assessment of Himalayan glacial lake changes using satellite observations  
788 from 1990 to 2015. *Remote Sensing of Environment*, 2017. 189(2): p. 1-13.

789 [25]. Brun, F., et al., Heterogeneous Influence of Glacier Morphology on the Mass Balance Variability in High  
790 Mountain Asia. *Journal of Geophysical Research: Earth Surface*, 2019. 124(6): p. 1331-1345.

791 [26]. Liu, Q., et al., Interannual flow dynamics driven by frontal retreat of a lake-terminating glacier in the Chinese  
792 Central Himalaya. *Earth and Planetary Science Letters*, 2020. 546: p. 116450.

793 [27]. Carrivick, J.L., et al., Toward Numerical Modeling of Interactions Between Ice-Marginal Proglacial Lakes  
794 and Glaciers. *Frontiers in Earth Science*, 2020. 8.

795 [28]. Huggel, C., et al., Remote sensing based assessment of hazards from glacier lake outbursts: a case study in  
796 the Swiss Alps. *Canadian Geotechnical Journal*, 2002. 39(2): p. 316-330.

797 [29]. Quincey, D.J., et al., Early recognition of glacial lake hazards in the Himalaya using remote sensing datasets.  
798 *Global and Planetary Change*, 2007. 56(1-2): p. 137-152.

799 [30]. Zhang, G., et al., An inventory of glacial lakes in the Third Pole region and their changes in response to  
800 global warming. *Global and Planetary Change*, 2015. 131: p. 148-157.

801 [31]. Gardelle, J., Y. Arnaud and E. Berthier, Contrasted evolution of glacial lakes along the Hindu Kush Himalaya  
802 mountain range between 1990 and 2009. *Global and Planetary Change*, 2011. 75(1-2): p. 47-55.

803 [32]. Chen, F., et al., Annual 30 m dataset for glacial lakes in High Mountain Asia from 2008 to 2017. *Earth  
804 System Science Data*, 2021. 13(2): p. 741-766.

805 [33]. Wang, X., et al., Changes of glacial lakes and implications in Tian Shan, Central Asia, based on remote  
806 sensing data from 1990 to 2010. *Environmental research letters*, 2013. 8(4): p. 44052.

807 [34]. Rick, B., et al., Dam type and lake location characterize ice-marginal lake area change in Alaska and  
808 NW Canada between 1984 and 2019. *The Cryosphere*, 2022. 16(1): p. 297-314.

809 [35]. How, P., et al., Greenland-wide inventory of ice marginal lakes using a multi-method approach. *Scientific  
810 Reports*, 2021. 11(1): p. 4481.

811 [36]. Ashraf, A., R. Naz and M.B. Iqbal, Altitudinal dynamics of glacial lakes under changing climate in the Hindu  
812 Kush, Karakoram, and Himalaya ranges. *Geomorphology*, 2017. 283: p. 72-79.

813 [37]. Roy, D.P., et al., Landsat-8: Science and product vision for terrestrial global change research. *Remote  
814 Sensing of Environment*, 2014. 145: p. 154-172.

815 [38]. Williamson, A.G., et al., Dual-satellite (Sentinel-2 and Landsat 8) remote sensing of supraglacial lakes in  
816 Greenland. *The Cryosphere*, 2018. 12(9): p. 3045-3065.

817 [39]. Paul, F., et al., Glacier shrinkage in the Alps continues unabated as revealed by a new glacier inventory from  
818 Sentinel-2. *Earth System Science Data*, 2020. 12(3): p. 1805-1821.

819 [40]. Zhang, M., F. Chen and B. Tian, An automated method for glacial lake mapping in High Mountain Asia  
820 using Landsat 8 imagery. *Journal of Mountain Science*, 2018. 15(1): p. 13-24.

821 [41]. Sheng, Y., et al., Representative lake water extent mapping at continental scales using multi-temporal  
822 Landsat-8 imagery. *Remote Sensing of Environment*, 2016. 185: p. 129-141.

823 [42]. Wang, J., Y. Sheng and Y. Wada, Little impact of the Three Gorges Dam on recent decadal lake decline  
824 across China's Yangtze Plain. *Water Resources Research*, 2017. 53(5): p. 3854-3877.

825 [43]. Wang, J., et al., Recent global decline in endorheic basin water storages. *Nature Geoscience*, 2018. 11(12):  
826 p. 926-932.

827 [44]. Wangchuk, S. and T. Bolch, Mapping of glacial lakes using Sentinel-1 and Sentinel-2 data and a random  
828 forest classifier: Strengths and challenges. *Science of Remote Sensing*, 2020. 2: p. 100008.

829 [45]. Zhao, W., et al., Lake area monitoring based on land surface temperature in the Tibetan Plateau from 2000  
830 to 2018. *ENVIRONMENTAL RESEARCH LETTERS*, 2020. 15(0840338).

831 [46]. Yao, X., et al., Definition and classification system of glacial lake for inventory and hazards study. *Journal*  
832 *of Geographical Sciences*, 2018. 28(2): p. 193-205.

833 [47]. Carrivick, J.L. and D.J. Quincey, Progressive increase in number and volume of ice-marginal lakes on the  
834 western margin of the Greenland Ice Sheet. *Global and Planetary Change*, 2014. 116: p. 156-163.

835 [48]. Carrivick, J.L. and F.S. Tweed, Proglacial lakes: character, behaviour and geological importance. *Quaternary*  
836 *Science Reviews*, 2013. 78: p. 34-52.

837 [49]. Li, D., D. Shangguan and M.N. Anjum, Glacial Lake Inventory Derived from Landsat 8 OLI in 2016 – 2018  
838 in China – Pakistan Economic Corridor. *ISPRS international journal of geo-information*, 2020. 9(5): p. 294.

839 [50]. Emmer, A. and V. Cuřin, Can a dam type of an alpine lake be derived from lake geometry? A negative result.  
840 *Journal of Mountain Science*, 2021. 18(3): p. 614-621.

841 [51]. RGI Consortium, Randolph Glacier Inventory – A Dataset of Global Glacier Outlines: Version 6.0:  
842 Technical Report. 2017: Global Land Ice Measurements from Space, Colorado, USA.

843 [52]. Rose, A., et al., LandScan Global 2020. 2021, Oak Ridge National Laboratory: Oak Ridge, TN.

844 [53]. Yao, C., et al., Temporal and Spatial Changes of Glacial Lakes in the China-Pakistan Economic Corridor  
845 from 1990 to 2018. *Journal of Glaciology and Geocryology*, 2020. 42(01): p. 33-42.

846 [54]. Ullah, S., et al., Observed changes in maximum and minimum temperatures over China- Pakistan economic  
847 corridor during 1980 – 2016. *Atmospheric Research*, 2019. 216: p. 37-51.

848 [55]. Kääb, A., et al., Contrasting patterns of early twenty-first-century glacier mass change in the Himalayas.  
849 *Nature*, 2012. 488(7412): p. 495-498.

850 [56]. Yao, T., et al., Different glacier status with atmospheric circulations in Tibetan Plateau and surroundings.  
851 *NATURE CLIMATE CHANGE*, 2012. 2(9): p. 663-667.

852 [57]. Hugonnet, R., et al., Accelerated global glacier mass loss in the early twenty-first century. *Nature*, 2021.  
853 592(7856): p. 726-731.

854 [58]. Hewitt, K., The Karakoram Anomaly? Glacier Expansion and the ‘Elevation Effect,’ Karakoram  
855 Himalaya. *Mountain Research and Development*, 2005. 25(4): p. 332-340.

856 [59]. Bolch, T., et al., Brief communication: Glaciers in the Hunza catchment (Karakoram) have been nearly in  
857 balance since the 1970s. *The Cryosphere*, 2017. 11(1): p. 531-539.

858 [60]. Azam, M.F., et al., Glaciohydrology of the Himalaya-Karakoram. *Science*, 2021. 373(6557): p. eabf3668.

859 [61]. Wulder, M.A., et al., Current status of Landsat program, science, and applications. *Remote Sensing of*  
860 *Environment*, 2019. 225: p. 127-147.

861 [62]. Nie, Y., et al., Glacial change in the vicinity of Mt. Qomolangma (Everest), central high Himalayas since  
862 1976. *Journal of Geographical Sciences*, 2010. 20(5): p. 667-686.

863 [63]. Jiang, S., et al., Glacier Change, Supraglacial Debris Expansion and Glacial Lake Evolution in the Gyirong  
864 River Basin, Central Himalayas, between 1988 and 2015. *Remote Sensing*, 2018. 10(7): p. 986.

865 [64]. Pfeffer, W.T., et al., The Randolph Glacier Inventory: a globally complete inventory of glaciers. *Journal of*  
866 *Glaciology*, 2014. 60(221): p. 537-552.

867 [65]. Sakai, A., Brief communication: Updated GAMDAM glacier inventory over high-mountain Asia. *The*  
868 *Cryosphere*, 2019. 13(7): p. 2043-2049.

869 [66]. Jarvis, A., et al., Hole-filled seamless SRTM data V4. 2008. 2008, International Centre for Tropical  
870 *Agriculture (CIAT): available from <http://srtm.csi.cgiar.org>.*

871 [67]. Farr, T.G., et al., The Shuttle Radar Topography Mission. *Reviews of Geophysics*, 2007. 45(2): p. RG2004.

872 [68]. Rabus, B., et al., The shuttle radar topography mission—a new class of digital elevation models acquired by  
873 *spaceborne radar. ISPRS Journal of Photogrammetry and Remote Sensing*, 2003. 57(4): p. 241-262.

874 [69]. Post, A. and L.R. Mayo, Glacier dammed lakes and outburst floods in Alaska: U.S. Geological Survey

875 Hydrologic Investigations Atlas 455. 1971, U.S. Geological Survey. p. 1-10.

876 [70]. Martín, C.N.S., et al., Proglacial landform assemblage in a rapidly retreating cirque glacier due to  
877 temperature increase since 1970, Fuegian Andes, Argentina. *Geomorphology*, 2021. 390: p. 107861.

878 [71]. Westoby, M.J., et al., Modelling outburst floods from moraine-dammed glacial lakes. *Earth-Science Reviews*,  
879 2014. 134: p. 137-159.

880 [72]. Chen, X., et al., Dam-break risk analysis of the Attabad landslide dam in Pakistan and emergency  
881 countermeasures. *Landslides*, 2017. 14(2): p. 675-683.

882 [73]. Wang, J., Y. Sheng and T.S.D. Tong, Monitoring decadal lake dynamics across the Yangtze Basin  
883 downstream of Three Gorges Dam. *Remote Sensing of Environment*, 2014. 152(0): p. 251-269.

884 [74]. Nie, Y., et al., Reconstructing the Chongbaxia Tsho glacial lake outburst flood in the Eastern Himalaya:  
885 Evolution, process and impacts. *Geomorphology*, 2020. 370(12): p. 107393.

886 [75]. McFeeters, S.K., The use of the Normalized Difference Water Index (NDWI) in the delineation of open  
887 water features. *International Journal of Remote Sensing*, 1996. 17(7): p. 1425 - 1432.

888 [76]. Cook, S.J. and D.J. Quincey, Estimating the volume of Alpine glacial lakes. *Earth Surf. Dynam.*, 2015. 3(4):  
889 p. 559-575.

890 [77]. Hanshaw, M.N. and B. Bookhagen, Glacial areas, lake areas, and snow lines from 1975 to 2012: status of  
891 the Cordillera Vilcanota, including the Quelccaya Ice Cap, northern central Andes, Peru. *The Cryosphere*, 2014.  
892 8(2): p. 359-376.

893 [78]. Lyons, E.A., et al., Quantifying sources of error in multitemporal multisensor lake mapping. *International*  
894 *Journal of Remote Sensing*, 2013. 34(22): p. 7887-7905.

895 [79]. Salerno, F., et al., Glacial lake distribution in the Mount Everest region: Uncertainty of measurement and  
896 conditions of formation. *GLOBAL AND PLANETARY CHANGE*, 2012. 92-93: p. 30-39.

897 [80]. Miles, E.S., et al., Glacial and geomorphic effects of a supraglacial lake drainage and outburst event, Everest  
898 region, Nepal Himalaya. *The Cryosphere*, 2018. 12(12): p. 3891-3905.

899 [81]. Liu, Q. and C. Mayer, Distribution and interannual variability of supraglacial lakes on debris-covered  
900 glaciers in the Khan Tengri-Tumor Mountains, Central Asia. *Environmental Research Letters*, 2015. 10(1): p.  
901 014014.

902 [82]. Wu, R., et al., A Deep Learning Method for Mapping Glacial Lakes from the Combined Use of Synthetic-  
903 Aperture Radar and Optical Satellite Images. *Remote Sensing*, 2020. 12(24): p. 4020

904 .

905